Global sensitivity analysis of uncertain parameters based on 2D modeling of solid oxide fuel cell

Chengru Wu[a], Meng Ni[b], Qing Du[a,*], Kui Jiao[a,*]

[a]State Key Laboratory of Engines, Tianjin University

135 Yaguan Road, Tianjin, China, 300350

[b]Building Energy Research Group, Department of Building and Real Estate

The Hong Kong Polytechnic University, Hung Hom, Kowloon, Hong Kong, China

*Corresponding authors: kjiao@tju.edu.cn (K. Jiao); duqing@tju.edu.cn (Q. Du)

tel: +86-22-27404460; fax: +86-22-27383362

Abstract

In this study, we propose an enhanced quasi-two dimensional and non-isothermal model for solid oxide fuel cell (SOFC) parametric simulation and optimization. The dependence of effective properties on microstructural parameters is fully considered in this model. Besides, an elementary effect (EE) approach based on Monte Carlo experiments is adopted to comprehensively evaluate the sensitivity of totally 24 parameters. A two sample Kolmogorov-Smirnov (K-S) test is carried out to evaluate the ability of EE method for robust and accurate sensitivity analysis. The investigation focuses on the important microstructural parameters of the composite anode/cathode function layers (AFL/CFL). With this research, relative volume fractions of conducting materials in the AFL/CFL are the most sensitive factors among all input parameters while particle radius is found to be the least sensitive microstructural parameters. The particle size ratio of electronic particles to ionic particles is found to be much more sensitive than particle size due to its significant effect on effective conductivity. The cathodic electrochemical parameters reflect cell performance more significantly than the anodic ones. To further elucidate the role of input factors, this study provides a principle for parametric sensitivity classification as well. Besides, impacts of current density variation on parametric sensitivity are comprehensively considered. Negative or positive effects of parameters on cell performance and their influencing mechanisms

are also discussed. Furthermore, global sensitivity analysis for single parameters at different positions is performed to assess the probability of structural optimization along the channel length. Then a feasible non-uniform distribution method in allusion to function layers is proposed for further improvement of cell performance according to global SA results of single parameters along the channel direction.

Key word: SOFC; Global sensitivity analysis; Elementary effect; Microstructure; Non-uniform.

Nomenclature

A	Cell geometric area (m^2)
C	Concentration (mol m^{-3})
D	Diffusion coefficient (m^2 s^{-1})
E_{act}	Activation energy (J mol^{-1})
E	Open circuit voltage (V)
F	Faraday's constant (C mol^{-1})
h	Surrounding heat transfer coefficient (W m^{-2} K^{-1})
i	Exchange current density (A m^{-2})
I	Current density (A m^2)
J	Electrochemical reaction rates (A m^{-3})
k	Pre-exponential factor
M	Molecular weight (kg mol^{-1})
p	Pressure (Pa)
R	Universal gas constant (J mol^{-1} K^{-1})
r_g	Hydraulic pore radius (μm)
r	Radius (μm)
δ	Thickness (μm)
T	Temperature (K)
q	Particle-radii ratio

S	Source term
ST	Stoichiometry ratio
V	Voltage (V)

Greek

λ	Three phase boundary length (m^{-1})
ρ	Density (kg m^{-3})
τ	Tortuosity
ε	Porosity
σ	Conductivity (S m^{-1})
β	Transfer coefficient
θ	Contact angle (º)
φ	Relative volume fraction
η	Overpotential (V)

Subscripts and superscripts

a	Anode
AFL	Anode function layer
ADL	Anode diffusion layer
BP	Bipolar plate
c	Cathode
CFL	Cathode function layer
CH	Channel
eff	Effective
ele	Electronic
ed	Electronic-conducting particle
el	Ionic-conducting particle
env	Environment
FL	Function layer
ion	Ionic
rev	reversible

TPB	Three phase boundary length
0	Standard state

1. Introduction

Solid oxide fuel cell (SOFC) is a promising energy conversion device with a lot of advantages such as flexible fuel choice, wide power range, low emission and high efficiency [1，2]. Despite those excellent features, extensive efforts are needed before successful commercialization of SOFC, for example, further SOFC performance improvement by design optimization of electrode structure. Compared with experimental investigation on cell structure optimization, numerical simulation and optimization can serve as a powerful, economic and reliable tool.

The operation of SOFC always involves complex physical/chemical phenomena such as multi-component diffusion, spontaneous reforming reaction and electrochemical reaction process. All these processes are highly coupled and usually behave nonlinearly. In addition, their geometric scale ranges from micro-scale to macro-scale. Empirical parameters are generally employed to ensure consistence of SOFC macroscopic behaviors such as the I-V curves between the numerical data and the experimental data, which is commonly used for model validation. In fact, empirical parameters that are hard to measure experimentally would inevitably increase model freedom degree thus damage the results reliability at the same time [3]. Thus, it is highly necessary to identify groups of factors that are most responsible for the results reliability and voltage fluctuation during the numerical predication process [4]. Modelers and practitioners have reached a consensus that sensitivity analysis (SA) method should be applied as a minimum, necessary component to answer the question of how uncertain of those factors are and where those uncertainties come from [5 - 7].

Sensitivity analysis is usually implemented in fuel cells to evaluate how uncertainties of inputs affect the predicted cell performance. Various methods have been proposed in recent studies. Most of published literatures on sensitivity analysis

of SOFC are dependent on ‘one-factor-at-a-time’ (OAT) method with the assumption of model linearity and additivity which is obviously irrational for most of multiple variables coupled computational models [8]. The biggest defect of OAT method is its incapability to reflect global impacts of entire parametric space on cell performance [9]. To overcome the inherent shortcomings of OTA method, a progressively increasing number of global sensitivity analysis techniques have been developed [10]. Wagner firstly proposed the idea of global sensitivity and meanwhile, a multi-component based global sensitivity analysis method was presented [11]. Sobol proposed a precise quantitative approach to evaluate the importance of input parameters with the assumption of independent input factors, while large computational resources would be needed to get the reliable results [12 - 14]. Hence it is not an applicable approach for computational models containing numerous parameters. Herschel et al. presented two types of high dimensional model representations (ANOVA/Cut HDMR) aiming at achieving a dramatic reduction of computational complexity for capturing input-output relationships and it was found that Cut HDMR shows significantly higher efficiency than ANOVA HDMR does [15]. Nevertheless, due to the negligence of input order correlating effects, HDMR method is unable to provide a description of model structure. Borgonove introduced a moment independent and variance-based global uncertainty indicator to evaluate parametric importance of independent parameters. With all input factors free to vary in their uncertain ranges, the computational stability is hard to guarantee, especially those multi-parameters coupling models [16]. Morris presented an effective screening global sensitivity measure and an efficient factorial sampling strategy to identify the importance of specific factors in multiple variance models. This method is dependent on the calculation of increasing ratio for each uncertain factors, namely elementary effect (EE). Average and variance value are obtained to evaluate overall sensitivity information of inputs [17]. To further enhance computational efficiency, Campolongo et al. further improved the EE method by raising new sampling strategy and refining the measure of absolute mean value of EE [18].

Even through sensitivity study has been extensively used in various scientific

researches, systematically global SA studies for SOFC are rarely found in the literatures. Chan et al. performed a sensitivity analysis focused on variation of cell layer thickness. Anode support fuel cells are found to be more efficient than cathode support ones under high pressure conditions [19]. Campanari and Iora established a finite volume SOFC model to conduct sensitivity analysis to elucidate the effects of different polarization losses with merely four empirical electrochemical parameters varied in a relatively wide range, thus demonstrated the importance of appropriate parameters [20]. Nagel et al. conducted a sensitivity analysis to gain insights of internal charge and mass process as well as performance fluctuation under different fuel compositions [21]. Based on an electrochemical model in which exchange current density and gas diffusion coefficients were completely dependent on cell microstructures, Ni et al. systematically analyzed the effects of structural/operational parameters on the individual overpotentials and operation efficiency of SOFC [22]. It should be noted that all the researchers of above literatures prefer "one-factor-at-a-time" sensitivity analysis (OAT-SA) method, in which all factors are assumed to be independent from one another while the interaction among factors are irrationally neglected. Moreover, recent studies of Vijay et al. proposed a two-stage validation strategy for SOFC model in which global sensitivity analysis were implemented to evaluated parametric uncertainties connected with the second kind of error [23]. Macroscopic operation parameters such as effective conductivity, heat transfer coefficient and diffusion coefficient were directly assigned to illustrate their uncertainties. However, above microscopic properties were determined by microstructural parameters to a great extent and actually not the original inputs for most of computational models [23]. In general, establishment of high computational efficiency model and adoption of appropriate sensitivity analysis techniques are the key factors to conduct the sensitivity analysis of SOFC.

In this study, a quasi-two dimensional and non-isothermal model with high computational efficiency is proposed to evaluate the parametric effects of SOFC. To the best of authors' knowledge, previous sensitivity studies are based on either isothermal assumption or non-isothermal model with simplified electrochemical process. Different from the previous studies, the mass transfer process along the channel direction are

taken into account in this study which are always neglected in sensitivity analysis in the literatures to simplify computation. A film percolation theory is implemented to evaluate effective mass and charge transport properties inside electrode. Elementary effects (EE) method which has been proved to be very promising for global sensitivity analysis with multiple input factors [24] is applied to evaluate the global sensitivity of totally 24 parameters. Totally 24 pivotal structural and empirical are selected to examine how and how much their variation affects cell performance. Then the coupling effects of different locations on cell performance are discussed. Based on the conclusions above, a feasible non-uniform distribution method in allusion to function layers is proposed for further improvement of cell performance.

2. Model development

2.1 Physical problem

The basic structure and computational domain of SOFC are illustrated in Figure 1, including the bipolar plate, channel, a thick Ni/yttria-stabilized zirconia (Ni/YSZ) anode diffusion layer (ADL), a thin Ni/scandium stabilized zirconia (Ni/ScSZ) anode function layer (AFL), a thin Ni/ScSZ cathode function layer (CFL) and a pure Ni/ScSZ electrolyte layer (ELE) in between. The directions both perpendicular to the channel and along the channel are treated as the major directions of mass and heat transfer. Electrochemical reaction merely occurs at the interface of three phase boundary (TPB) area. Owing to particular aspect ratio of SOFC, namely thin electrode thickness but large channel length, a quasi-two dimensional model is proposed in this study which couples the 1D heat and mass transfer process through electrode and the 1D transport process along the channel direction [25]. This is a popular method since it provides the distributions of current density, species and temperature distributions in two directions with manageable computational resources compared with traditional 3D model. It is essential to remark that the quasi-two dimensional model here is not like

the traditional segment models that simply integrate specific number of 1D model and connect them by the channel flow. The mass and heat transfer phenomena as well as charge transport process inside electrode and channel are integrated together to capture the real physical process along the channel direction to a great extent. Detailed geometry and operating conditions of a basic case are shown in Table 1 [26 - 29].

Model assumption

(1) The gas velocity along the flow channel is regarded as constant.

(2) Ideal gas law is considered.

(3) The gas flow in the channel is dominated by convection and the diffusion process is neglected.

(4) The pressure loss along the channel direction is small and can be neglected.

(5) Contact resistance between two adjacent layers is ignored.

(6) The radiation heat transfer inside the fuel cell is not considered.

(7) Flow is in steady state and laminar inside channel.

2.2 Conservation equations

2.2.1 Mass transport in channel

In this model, the pressure drop is safely neglected due to relatively short channel and small Reynold's number. The assumption above simplifies the model a lot by avoiding complicated momentum equation solving process with great numerical accuracy. Then the mass conservation equation can be described as:

$$u_y \frac{\partial C_{i,\text{channel}}}{\partial y} = \kappa_i \frac{I}{n_i F \delta_{\text{channel}}} \tag{1}$$

where $C_{i,\text{channel}}$ (mol m^{-3}) represents the gas concentration of species i along the channel, κ_i is the stoichiometric coefficient (1 for H_2 and O_2, -1 for H_2O), n_i is the charge transfer number of species i, and I (A m^{-2}) refers to the current density distribution along the channel. u_y (m s^{-1}) represents the flow velocity which depends on stoichiometric ratio and operating current density:

$$u_y = ST \frac{I_0 A_{\text{act}}}{2FC_{\text{inlet},i} A_{\text{inlet}}} \tag{2}$$

where ST is the stoichiometric ratio and I_0 (A m^{-2}) is the operating current density. F is the Faraday's constant (96,458 C mol^{-1}).

Sherwood number (Sh) is introduced to describe the gas transport process from channel to porous interface in analogy with heat transfer process. The interfacial concentration at electrode interface can be expressed as:

$$C_{i,\text{interface}} = C_{i,\text{channel}} - \frac{IA_{\text{act}}}{2ShD_{\text{eff},i} F d_{\text{h}} A_{\text{inlet}}} \tag{3}$$

where $D_{eff,i}$ (m^2 s^{-1}) is the effective diffusion coefficient in channel. d_{h} (m) is hydraulic diameter of channel.

2.2.2 Mass transfer in electrode

Diffusion processes in both directions are considered while the convection effects are small in the porous electrodes and can be reasonably neglected. Then the mass diffusion process in electrode is formulated as:

$$D^x_{\text{eff},i} \frac{\partial^2 C_i}{\partial x^2} + D^y_{\text{eff},i} \frac{\partial^2 C_i}{\partial y^2} = S_i \tag{4}$$

where S_i (mol m^{-3} s^{-1}) represents the source terms of species i which are comprehensively listed in Table 2. $D^x_{\text{eff},i}$ (m^2 s^{-1}) and $D^y_{\text{eff},i}$ (m^2 s^{-1}) are the effective diffusion coefficients in two directions, respectively, which is calculated by Bosanquet equation [30] and the detailed computational formula are summarized in Table 3 [30].

2.2.3 Energy balance

The energy balance equation is solved over the entire fuel cell domain. As the convection in the porous electrode is neglected, the governing equation of temperature distribution is expressed as:

$$k_{\text{eff}}^{x}\frac{\partial^2 T}{\partial x^2}+k_{\text{eff}}^{y}\frac{\partial^2 T}{\partial y^2}=S_T \tag{5}$$

where k_{eff}^{x} (W m^{-2} K) and k_{eff}^{y} (W m^{-2} K) represent the effective thermal conductivity in two directions. T (K) is the temperature, and S_T (W m^{-3}) is the source term of heat transport that is listed in Table 2. The heat exchange between fuel cell and surrounding environment can be expressed as [28]:

$$Q=hA_{\text{wall}}(T_{\text{wall}}-T_{\text{env}}) \tag{6}$$

where h (W m^{-2} K) represents the convective thermal coefficient.

2.3 Electrochemical model

The output voltage is described as:

$$V_{\text{out}}=E_{\text{rev}}-\eta_{\text{act}}-\eta_{\text{ohm}} \tag{7}$$

where V_{out} (V) represents the output voltage. η_{act} (V) is the total activation loss and η_{ohm} (V) is the total ohmic loss. E_{rev} (V) is the reversible voltage following thermodynamic principles and can be evaluated using Nernst equation [28]:

$$E_{\text{nernst}}=1.253-2.4516\times10^{-4}T-\frac{RT}{2F}\ln\left(\frac{p_{\text{H}_2\text{O}}}{p_{\text{H}_2}p_{\text{O}_2}^{0.5}}\right) \tag{8}$$

where R is the universal gas constant (8.314 J mol^{-1} K^{-1}). $p_{\text{H}_2\text{O}}$, p_{H_2} and p_{O_2} (Pa) represent partial pressures of water vapor, hydrogen and oxygen, respectively. The concentration overpotential is included in the reversible voltage as the particle pressure is obtained by multiplying the operating pressure and species mole fraction at the reaction site.

The ohmic loss caused by charge transfer resistance is calculated by ohm's law:

$$\eta_{\text{ohm}}=(R_{\text{BP, a/c}}+R_{\text{ADL, a}}+R_{\text{FL, a/c}}+R_{\text{CH, a/c}}+R_{\text{ELE}})I \tag{9}$$

Where η_{ohm} represents ohmic activation. $R_{\text{BP, a/c}}$, $R_{\text{ADL, a}}$, $R_{\text{FL, a/c}}$, $R_{\text{CH, a/c}}$ and R_{ELE} refer to the conductivity resistance for different parts of SOFC. I is the local current density distribution.

The Butler-Volmer (B-V) equation illustrates the relationship between electrochemical reaction rates and activation loss. As there is only an average gas concentration corresponding to each FL segment, average activation loss at middle FL can be calculated by an inverse function of B-V equation under a constant current density mode [28]:

$$J_{\mathrm{a}} = i_{0,\mathrm{a}} \lambda_{\mathrm{tpb}}^{\mathrm{eff,a}} \left(\exp\left(\frac{2\beta_{\mathrm{a}} F \eta_{\mathrm{act,a}}}{RT} \right) - \exp\left(-\frac{2(1-\beta_{\mathrm{a}}) F \eta_{\mathrm{act,a}}}{RT} \right) \right) \tag{10}$$

$$J_{\mathrm{c}} = i_{0,\mathrm{c}} \lambda_{\mathrm{tpb}}^{\mathrm{eff,c}} \left(\exp\left(-\frac{4\beta_{\mathrm{c}} F \eta_{\mathrm{act,c}}}{RT} \right) - \exp\left(\frac{4(1-\beta_{\mathrm{c}}) F \eta_{\mathrm{act,c}}}{RT} \right) \right) \tag{11}$$

where J_{a} (A m^{-3}) and J_{c} (A m^{-3}) represent the electrochemical reaction rates while the corresponding current density can be obtained by multiplying thickness of function layer. $\lambda_{\mathrm{tpb}}^{\mathrm{eff,a}}$ and $\lambda_{\mathrm{tpb}}^{\mathrm{eff,c}}$ (m^2 m^{-3}) refers to effective three phase boundary length of anode and cathode. $i_{0,\mathrm{a}}$ and $i_{0,\mathrm{c}}$ (A m^{-2}) are the reference exchange current density in anode and cathode sides which are calculated by the following formulas [29]:

$$i_{0.\mathrm{a}} = k_{0,\mathrm{a}} \left(\frac{C_{\mathrm{H_2,\,b}} RT}{p_0} \right)^{\gamma_{\mathrm{H_2}}} \left(\frac{C_{\mathrm{H_2O,\,b}} RT}{p_0} \right)^{\gamma_{\mathrm{H_2O}}} \exp\left(-\frac{E_{\mathrm{act,a}}}{R} \left(\frac{1}{T} - \frac{1}{T_{\mathrm{ref}}} \right) \right) \tag{12}$$

$$i_{0.\mathrm{c}} = k_{0,\mathrm{c}} \left(\frac{C_{\mathrm{O_2,\,b}} RT}{p_0} \right)^{\gamma_{\mathrm{O_2}}} \exp\left(-\frac{E_{\mathrm{act,c}}}{R} \left(\frac{1}{T} - \frac{1}{T_{\mathrm{ref}}} \right) \right) \tag{13}$$

where $k_{0,\mathrm{a}}$ and $k_{0,\mathrm{c}}$ are the pre-exponential factors in the cause of fitting experiment data, and $E_{\mathrm{act,a}}$ and $E_{\mathrm{act,c}}$ (J mol^{-1}) represent the active energy for anodic and cathodic electrochemical reaction. $\gamma_{\mathrm{H_2}}, \gamma_{\mathrm{H_2O}}$ and $\gamma_{\mathrm{O_2}}$ represent the reaction order of H_2, H_2O and O_2, respectively.

For simplification, the control volume along the channel length is regarded as parallel hence the potential of bipolar plate interface remains the same. Different gas concentration and temperature distribution along the channel direction result in a variation of current density distribution. Under the constant current density mode, the value of output voltage and local current density distribution can be solved based on the following system of nonlinear equations [31]:

$$\begin{cases} 0 = E_{\text{rev}}^{[0]} - V_{\text{out}} - I^{[0]}R^{[0]} \\ 0 = E_{\text{rev}}^{[n]} - V_{\text{out}} - I^{[n]}R^{[n]} \ldots \\ 0 = E_{\text{rev}}^{[N\text{-}1]} - V_{\text{out}} - I^{[N-1]}R^{[N-1]} \ldots \\ \dfrac{\sum_{n=0}^{n=N-1} I^{[n]}}{N} = I \end{cases} \tag{14}$$

where $E_{\text{rev}}^{[n]}$, $I^{[n]}$ and $R^{[n]}$ represent the reversible voltage, current density and total resistance of n th segment;

2.4 Film percolation microstructure model

In this section, an improved film percolation model is applied to investigate the effective characteristics of microstructures [32, 33]. Porous structures are assumed to consist of random mixture of spherical electronic and ionic conducting particles in this theory. By changing primary microstructural parameters, including average particle radius, particle radii ratio, relative electronic/ionic volume fraction as well as porosity, the basic characteristics of microstructures can be significantly affected. Several important effective properties estimated by percolation theory are listed below:

Three phase boundary length

Active three-phase boundary length is actually formed with percolated clusters and pores. There are two types of percolated clusters thought to be conductive in the composite electrode, namely cluster I and cluster II [31, 32]. The active three phase boundary (TPB) length is dependent on the probability of particle that belongs to cluster I and II, namely percolated probability which can be calculated as [32, 33]:

$$P_{\text{I},k} = \left[1 - \left(\frac{3.764 - Z_{k,k}}{2} \right)^{2.5} \right]^{0.4} \tag{15}$$

$$P_{\text{II},k} = \left(1 - P_{\text{I},k}\right) \left[\beta \frac{Z_{k,k}}{\overline{Z}} (1 - P_{\text{I},k})^{\gamma} \right]^{\alpha(N-1)} \tag{16}$$

where $Z_{k,k}$ is the average number of contacts. Then the total probability is [32, 33]:

$$P_k = P_{\text{I},k} + P_{\text{II},k} \tag{17}$$

The total TPB length can be estimated as [32]:

$$\lambda_{\mathrm{tpb}}^{\mathrm{eff}} = l_{\mathrm{ed,el}} n_{\mathrm{ed}}^{\mathrm{v}} Z_{\mathrm{ed,el}} P_{\mathrm{ed}} P_{\mathrm{el}} = l_{\mathrm{el,ed}} n_{\mathrm{el}}^{\mathrm{v}} Z_{\mathrm{el,ed}} P_{\mathrm{ed}} P_{\mathrm{el}} \tag{18}$$

where $l_{k,l}$ is the contact perimeter between two types of contacting particles, $Z_{k,l}$ is the coordination number [32].

$$l_{k,l} = 2\pi \min(r_k, r_l) \sin\theta \tag{19}$$

$$Z_{k,l} = 0.5(1 + r_k^2 / r_l^2)\overline{Z} \frac{\psi_l / r_l}{\sum_{k=1}^{2} \psi_k / r_k} \tag{20}$$

Effective conductivity

Effective conductivity of electronic and ionic conducting materials can be estimated as [32]:

$$\sigma_k^{\mathrm{eff}} = \sigma_{\mathrm{k}}^0 \left(\frac{\psi_k - \psi_k^t}{1 + \varepsilon / (1-\varepsilon) - \psi_k^t} \right)^2 \tag{21}$$

where $\psi_{\mathrm{k}}^{\mathrm{t}}$ represents the percolation threshold volume fraction, which can be calculated by equations set [32]:

$$\overline{Z} \frac{\psi_{\mathrm{ed}}^t}{\psi_{\mathrm{ed}}^t + (1 - \psi_{\mathrm{ed}}^t) q} = 1.764 \tag{22}$$

$$\overline{Z} \frac{\psi_{\mathrm{el}}^t}{\psi_{\mathrm{el}}^t + (1 - \psi_{\mathrm{el}}^t) / q} = 1.764 \tag{23}$$

$\overline{Z}$ equals to 6 here, and q represents the particle radii ratio. The pure conductivity can be calculated as follows [28]:

$$\sigma_{\mathrm{ScSZ}}^0 = 6.92 \times 10^4 \exp\left(\frac{-9681}{T} \right) \tag{24}$$

$$\sigma_{\mathrm{LSM}}^0 = \frac{4.2 \times 10^7}{T} \exp\left(\frac{-1150}{T} \right) \tag{25}$$

$$\sigma_{\mathrm{YSZ}}^0 = 3.34 \times 10^4 \exp\left(\frac{-10300}{T} \right) \tag{26}$$

$$\sigma_{\mathrm{Ni}}^0 = 3.27 \times 10^6 - 1065.3T \tag{27}$$

Hydraulic pore radius

The hydraulic pore radius in electrode is determined by microstructure of conductive materials [32]:

$$r_g = \frac{2}{3\left(\psi_{ed}/r_{ed} + \psi_{el}/r_{el}\right)\left(1-\varepsilon\right)} \tag{28}$$

2.5 Elementary effects method

In this section, elementary effects approach proposed by Morris is introduced to perform global sensitivity analysis [18]. For simplification, cell performance is regarded as the function of total k input factors:

$$V = f\left(X_1, X_2, ..., X_n, ..., X_k\right) \tag{29}$$

where $X_1, X_2, \ldots, X_k$ represent the standardized input variables that ranges from 0 to 1. Each standardized variable is discretized into L levels. The conversion relationship between the actual value and no dimensional value can be estimated as [18]:

$$s_i = X_i\left(s_{max} - s_{min}\right) + s_{min} \tag{30}$$

where s_i represents the real value of input factors. Then a sample space of k dimensional and L level is constructed. Elementary effects for i th input factors is defined as [18]:

$$EE_i = \frac{f\left(X_1, X_2, ...X_i \pm \Delta, ...X_k\right) - f\left(X_1, X_2, ...X_i, ...X_k\right)}{\pm\Delta} \tag{31}$$

where EE_i represents the elementary effects involving with two groups of parameters which is obtained from sample space randomly. Each parameter range is evenly divided into L portions while $\triangle$ takes the value of $L/2(L\text{-}1)$ to ensure equal probability during the sampling process. In order to ensure that the selected sampling points could cover the whole sampling space, Morris proposed a randomized sampling strategy to get the sampling matrix [18]:

$$B^* = \left(J_{k+1,1}x^* + \Delta B\right)P^* \tag{32}$$

$$\Delta B = \left(\Delta / 2\right)\left[\left(2B - J_{k+1,k}\right)D^{*} + J_{k+1,k}\right] \tag{33}$$

where B^{*} is a $(k+1)\times k$ sampling matrix in which each row represents a k-dimensional sampling point corresponding to one elementary effects factor. $J_{k+1,1}$ refers to a $(k+1)\times 1$ matrix of 1' s, while $J_{k+1,k}$ refers to a $(k+1)\times k$ matrix of 1' s. P^{*} represents a random permutation matrix that each row and column only has one entry of 1 and 0's elsewhere. D^{*} is a diagonal matrix of -1's and 1's with equal probabilities which determines the increase or decrease of factors along the trajectory. B is a $(k+1)\times k$ matrix of 0's and 1's with the limitation that two rows of B only differ in their i th value [18]:

$$B = \begin{bmatrix} 0,\ 0,\ 0,\ ...0 \\ 1,\ 0,\ 0,\ ...0 \\ 1,\ 1,\ 0,\ ...\ 0 \\ ... \\ 1,\ 1,\ 1,\ ...\ 1 \end{bmatrix} \tag{34}$$

The sampling strategy above merely corresponds to one randomly generated trajectory. There are r trajectories selected to obtain r elementary effects for each factor. By averaging these elementary effects of each factor, the sensitivity of factor i can be evaluated using formulas set [18, 19]:

$$\mu_i = \frac{1}{r}\sum_{j=1}^{r} EE_i^{j} \tag{35}$$

$$\mu_i^{*} = \frac{1}{r}\sum_{j=1}^{r}\left|EE_i^{j}\right| \tag{36}$$

$$\sigma_i^{2} = \frac{1}{r-1}\sum_{j=1}^{r}\left(EE_i^{j} - \mu\right)^{2} \tag{37}$$

where μ_i, μ_i^{*} and σ^2 refer to the mean value, absolute mean value and sampling variance of elementary effects.

3. Result and discussion

3.1 Solution procedures and experiment validation

The computational process is implemented by in-house codes based on Matlab platform. There are totally 8×10 nodes defined in the entire computational domain while finite difference method and fourth-order Runge-Kutta approach are utilized to discretize and solve the governing equations with a numerical precision of 10^{-8}.

Figure 2 shows the comparison between modelling prediction and experiment data [34]. Humidified hydrogen (96%) is supplied as fuel to the anode. Air is used in cathode. Effects of temperature distribution (1023/1073/1123 K) are taken into account as well. Both the global polarization curves and various voltage losses show reasonable agreement with experiment data although there still exists slight inconformity of polarization curve at 1023 K. This small difference between modeling results and the experimental data might result from inaccurate experimental measurements or the use of several assumptions in the model. It worth to point out that this study focuses on the global sensitivity of input parameters under the normal working conditions, while some extreme working condition such as extreme current density is not taken into account. Duo to the fact that fuel or oxygen starvation cause divergence, the output voltage of this model cannot go down to 0V [35].

Moreover, careful evaluation is necessary to ensure that global sensitivity approach is reliable and applicable. A two sample Kolmogorov-Smirnov (K-S) test is employed to validate the computational stability of SA method by examining whether two independently calculated results have notable difference. The Kolmogorov-Smirnov statistics for two given cumulative distribution function $G(x)$ is:

$$D = \sup\left|G_i(\text{Result } j)\text{-}G_i(\text{Result } k)\right| \tag{38}$$

where $G_i(\text{Result } j)$ and $G_i(\text{Result } k)$ represent the absolute distribution of elementary effects for two independently calculated results. D represents the standard deviation. Two randomly selected cases are compared with standard case 1 under exactly same conditions. There is no space to go into detail for all factors. An example of CFL particle radius is plotted in Figure 3 (a) and (b). The p-value is treated as a criteria to judge whether the result is credible. Larger p-value than significant level 0.05 is desirable result as it indicates the stability and reliability of the calculation

results. As can be seen from Figure 3 (a) and (b), p-value of each plot is much higher than 0.05, hence the sensitivity analysis scheme is accurate.

3.2 Global sensitivity analysis

3.2.1 The necessity to do sensitivity analysis

There are three cases summarized in Table 4 to demonstrate the necessity to do global sensitivity analysis. Several parameters are defined to be different among these cases. Case 2 has absolutely different structural parameters compared with cased 1 while case 3 has different empirical parameters and relative volume fraction compared with case 1 and case 2. As can be seen from Figure 4, there are two main evidences that emphasize the importance to conduct sensitivity analysis. On the one hand, we can see that different combinations of parameters may result in identical polarization curves, which arises the problem that polarization curves sometimes are insufficient for validation. On the other hand, parametric variation amplitudes among three cases are quite different. For instance, when we compare case 3 with case 1, as relative volume fractions decrease by 10%, the pre-exponential factors change more than tenfold to fit the I-V curve, which signifies that the importance of different parameters on cell performance are diverse, and obviously, positive or negative effects of parameters are different as well.

In this study, a global sensitivity analysis of totally 24 input parameters is performed based on an elementary effects method. Sensitive properties of input factors and their immanent causes are comprehensively investigated. To further explore the potential of microstructure optimization, sensitivity examinations for single parameters at different position along the channel length are also conducted in the last segment.

3.2.2 Sensitivity analysis of diverse input parameters

In this section, totally 24 widely used parameters in SOFC models are selected to examine how and to which extent their variation affects cell performance, while the

coupling effects of those factor are also considered in this section. In previous sensitivity analysis literatures, input parameters are always irregularly enlarged to adapt more working conditions [36]. Such procedures have hidden dangers that wide range of parameters itself can also greatly impact the cell performance while effects of interactions among all parameters might be completely or partly covered. As different selected ranges of parameters might significantly influence sensitive degree, input parameters are defined to fluctuate around the standard value with a unified wave range of ±15%, which are listed in Table 5. Current density of 1500 A m^{-2} and 7500 A m^{-2} are selected as the basic operating condition in this study.

For a more comprehensive study of parametric sensitivity, particle radii ratio (q) is employed to describe the relative size of electronic particle radius (r_{ed}) and ionic particle radius (r_{el}). r_{ed} is defined as the input variable to reflect the overall effects of particle size while r_{el} varies as particle radii ratio changed. Theoretically, particle radii ratio does not merely refer to effects of ionic particle radius but also represents impacts of relative size of electronic and ionic particle radius, which can be expressed as:

$$q = \frac{r_{ed}}{r_{el}} \tag{39}$$

We demonstrate nominal value of particle radii ratio as 1 aimed at two main tasks: (1) To obtain a reasonable range of particle radii ratio including both less than 1 part and larger than 1 part. (2) To get a relatively wide value space of relative volume fraction owing to the facts that too large particle radii ratio would greatly narrow effective range of relative volume fraction [30].

Researchers generally reach a consensus that a multi-layer anodic structure should be proposed to enable an anode function layer (AFL) to restrain active loss by maximizing effective TPB length [37]. Microstructure design of function layers is supposed as one of the fundamental challenges for electrode optimization [34]. In this regard, sensitivity analysis of microstructural parameters inside FL shows guiding significance both on the structural optimization and model improvement. It is natural that parametric sensitivity analysis for function layers is taken into consideration in the first section.

Sensitivity characteristics for microstructural factors at AFL/CFL are illustrated in Figure 5(a) - (d) with the distribution properties of three specific sensitivity measurement factors, μ and μ^* and σ^2. A basic condition of 1500 A m^{-2} is discussed as an example while the sensitive characteristics are compared with an operating condition of 7500 A m^{-2}. It is important to point out that relative volume fractions at AFL/CFL sides are the most sensitive factors in the light of largest value of both μ^* and σ^2. Ohmic overpotential is the essential factor governing the sensitivity of relative volume fraction. More significant parametric variation effects of particle radii ratios on cell performance than electronic particle radius should be noted. Moreover, particle radius at AFL side exhibits the lowest importance on cell performance considering both mean value and sample variance of EE. Activation loss plays a major role for insensitivity of electronic particle radius. Considering that electronic and ionic particle radius contribute same proportion to active overpotential by influencing effective TPB length, it is concluded that sensitivity of particle radii ratio largely involves with ohm loss. In other words, small ionic particle radius shows more significant influence than small electronic particle radius does by way of influencing effective conductivity.

Electronic particle radius at CFL shows larger impacts on cell performance than that of AFL side. A vital mechanism contributing to the sensitivity of electronic particle radius at CFL is relatively small oxygen reaction rates. It is interesting to find that thickness of both side is not that important as expected. In view of analyses above, the microstructural factors should be given higher priority than FL thickness in electrode optimization.

Even through there is an impressive improvement of sensitivity at 7500 A m^{-2} compared with 1500 A m^{-2}, relative sensitivity sequence among different factors seems does not change. To further characterize the effects of current density variation, Figure 6 (a) - (d) exhibit a comparison of different geometric parameters at both sides. Considering that sensitivity variation tendencies of several parameters slightly fluctuate at high current density, a fitting curve method is applied here to clarify the sensitivity variation tendency. Sensitivities of thickness, relative volume fraction and particle radii ratio show almost linear growth with the increase of current density. Sensitivity

disparities between several AFL and CFL factors, including relative volume fraction and particle radii ratio, gradually widened at high operating current density while increase of current density, to some extent, promote the sensitivity consistency between AFL and CFL thickness. Differently, with increasing current density, impact of particle radius at CFL remains almost unchanged while sensitivity of particle radius at AFL still remains far less than that of CFL.

Figure 7 (a) - (d) present sensitivity properties for the rest of vital geometric parameters. Although electrolyte thickness ranks the third most sensitive factor among this group of parameters, the value of μ^* and σ^2 are merely a bit bigger than the least sensitive factors in the function layers. Sherwood number is always employed to measure the proportion of convection and diffusion process from channel to electrode interface and it is found that its impact on performance is not as significant as expected. Sensitivity of tortuosity, which largely involves with diffusion resistance, is much lower than porosity on account of low diffusion loss in the porous electrode. Porosity is found to be the most sensitive factor in this group owing to the facts that porosity is not only related to diffusion resistance but also tightly affects the effective TPB length and conductivity. Collectively, these facts and speculations reveal that the nature of porosity optimization for SOFC is to acquire appropriate effective properties of TPB length and conductivity while diffusion coefficient can be regarded as the secondary factor. Considering that the entire effective reaction area and most of charge resistance exist in function layers, above investigation unmasks a dominating effect of function layers on overall sensitivity of porosity.

Sensitive characteristics of electrochemical parameters are plotted in Figure 7 (e) - (h). Reaction order and pre-exponential factor at cathode side are the most sensitive empirical factors while active energy of both side show minimal effects considering average and variance value of EE. Not surprisingly, empirical factors in cathode affect cell performance more significantly on account of much lower electrochemical reaction rate of O_2. Notable increase of sensitivity is observed at 7500 A m^{-2} compared with that of 1500 A m^{-2}.

Sensitivity tendencies for several high sensitivity factors towards increase of

current density are illustrated in Figure 8 (a) and (b). Sensitivities of geometric and pre-exponential factor at anode side show approximately linear growth as operating current density rising. Duo to the limitation of oxygen diffusion rates, sensitivities of O_2 reaction order as well as cathodic pre-exponential factors gradually tend to be flat at high current density.

Figure 9 exhibits the histogram distribution of μ and μ^* to better understand the sensitivity properties of input parameters. Negative value of μ means negative effects on cell performance. Histogram lengths of μ and μ^* are utilized as the standard to judge the monotonicity of parameters. Exactly same histogram heights of μ and μ^* mean monotonous effects while different heights correspond to non-monotonous effects on cell performance. Except that increase of particle radii ratios improves the cell performance, all the rest of microscopic parameters in function layers exhibit monotonous negative impacts on cell voltage. Due to the presence of more significant mass transfer and charge transport resistance, increase of layer thickness shows a negative effect on cell performance in most cases. By affecting active polarization, pre-exponential factors show monotonous positive effects while reaction orders of gas species work in the opposite direction.

According to the sensitivity measurement factor μ^*, uncertain parameters are clarified into very sensitive factors, rather sensitive factors and insensitive factors in terms of principles below:

$\mu^*>0.017$ very sensitive factors

$0.005<\mu^*<0.017$ rather sensitive factors

$\mu^*<0.005$ insensitive factors

Detailed classifications are listed in Table 6. The Monte-Carlo approach is applied to validate the accuracy and reliability of numerical model and sample strategy. As can be seen in Figure 10, all factors, sensitive factors and insensitive factors are individually tested 1200 times. Sensitive factors result in an identical voltage distribution area with all factors while voltage range produced by insensitive factors is very narrow compared with that of all factors. It is clear that sensitive factors are the primary causes for fluctuation of cell performance hence great efforts are needed

on optimizing those truly sensitive factors rather than insensitive ones. It should be demonstrated that the model is efficient enough to conduct global sensitivity analysis. The computational time of one global sensitivity analysis process is about 5 minutes. The operation of Monte-Carlo approach takes longer time since all factors, sensitive factors and insensitive factors are individually tested 1200 times and this process takes about 1 hours.

3.2.3 Sensitive analysis for single parameters along the channel length

In the previous section, totally 24 parameters have been classified into sensitive and insensitive factors based on EE method. Microstructural parameters in the function layers have been proven to be most sensitive for cell performance. In the following work, global sensitivities of single parameters at FL along the channel direction are tested using EE method to assess the probability of structural optimization along the channel length. In contrast to the previous sampling strategy, single parameters at different positions are regarded as independent factors to investigate the coupling effects of different locations on cell performance in this approach. Cell structure is divided into ten segments along the channel to obtain a 11×10 sampling matrix, each row of which represents a non-uniform distribution of the specific structural parameters while the other parameters remain unchanged. In a nutshell, a combination of EE and OAT method is applied to evaluate the significance of specific parameters at different locations.

Duo to the facts that sensitivity distribution regularities of AFL are quite similar with that of CFL, sensitivities of anodic parameters are plotted as an example to exhibit the impacts of position on cell performance in Figure 11 (a) - (d). Apparently different sensitivities of single parameters at different position lie in an interaction of temperature and species distribution along the channel length. It can be seen from Figure 11 that the highest sensitivity is obtained at the location near the center. The counter-flow operation has the advantage in power output and the temperature near the center achieves peak [38, 39], which significantly influences effective conductivity,

reversible voltage and exchange current density. Theoretically, these properties are essential factors governing cell performance that is also greatly affected by microstructural parameters. The combined effects of temperature and microstructural parameters acting together amplify the sensitivity of different location on voltage fluctuation.

In conclusion, investigation carried out above has further revealed a feasible microstructural optimization method along the channel direction, namely non-uniform distribution of microstructure factors. The core mechanism of this approach is placed on the construction of non-uniform distribution along the channel length in terms of SA results.

3.3 Non-uniform microstructure distribution along the channel length

According to the approximately parabolic tendency of sensitivity distribution along the channel length, we design an uneven distribution strategy for microscopic parameters in the function layers where microstructure parameters are distributed in a parabolic pattern as shown in Figure 12 (a). The non-uniform distribution strategy for microscopic parameters can be formulated as:

$$P = -\frac{4S_N(\chi+\omega)}{L_{\text{cell}}^2}\left(x-L_x\right)^2 + S_N\left(1+\chi\right) \tag{39}$$

$$N = \frac{4S_N(\chi+\omega)}{L_{\text{cell}}^2}\left(x-L_x\right)^2 + S_N\left(1-\omega\right) \tag{40}$$

where S_N represents nominal parameters as mentioned before. χ and ω are introduced to specify upper and lower limits of parameters. P and N express the distribution strategy for positive and negative effect factors. L_x represents the extreme parabola coordinates. Three selected cases with different χ and ω are listed in Table 7. Case 4 represents uniform distribution. Case 5 refers to a non-uniform distribution with same value of χ and ω while case 6 chooses different values of χ and ω. L_x equals $L_{\text{cell}}/2$ here. Examples of optimized non-uniform distribution for microscopic factors are illustrated in Figure 12 (b), the voltage output of which are compared with that of

uniform distribution. Attention should be paid to the findings of this investigation that sensitivity analysis is employed as only basis for non-uniform structural optimization. We can see that there is an obvious improvement of cell performance when non-uniform distribution is utilized along the channel length.

The positive or negative effects of χ and ω are dependent on their corresponding parameters. For negative effect factors, larger value of ω and smaller value of χ are beneficial to performance improvement. For negative effect factors, smaller value of ω and larger value of χ are suitable. However, overall ranges of χ and ω are limited owing to coupling effects among parameters for forming an effectively conductive connection. Choosing appropriate value of χ and ω is essential for structural optimization along the channel length.

Evidently, structural optimization focusing on high sensitivity position is more efficient than equivalent optimization of all locations. It is confirmed that non-uniform distribution approach based on sensitivity analysis rewards more attention in future research.

4. Conclusion

In this study, a computationally efficient quasi-two dimensional model is developed, considering detailed heat and mass transfer as well as electrochemical process in both directions, which are not fully considered in previous sensitivity analysis of SOFC. An elementary effects approach proposed by Morris and improved by Campolongo is employed in this paper to conduct global sensitivity analysis of totally 24 input parameters. By creatively combining EE and OAT approach together, sensitivity distribution of single parameters along the channel direction are also evaluated. This study is designed to process an elementary effects method to conduct global sensitivity analysis and explain how uncertainties of input factors impact cell performance and the conclusions are listed as follows:

1. Microstructural parameters of anode and cathode function layers play a decisive role in fuel cell performance with 7 very sensitive factors. Relative

volume fraction of conductive materials is found to be most sensitive factors while particle radius at AFL exhibits lowest importance on cell performance among microscopic factors. Ionic particle radius is much more sensitive than electronic particle radius by means of influencing effective conductivity rather than TPB length. Almost all cathode side factors contribute more to voltage fluctuation than anode side factors. Function layer thickness is not that important as expected, hence it is suggested that further study should concentrate on microstructure optimization.

2. Impacts of current density variation on sensitivity are also observed in this study. Except that most factors increase linearly as current density growing, variation tendencies of particle radius and other empirical parameters at cathode side gradually become flat owing to the limitation of O_2 diffusion rates.
3. Seven microstructural parameters are classified into very sensitive factors. Five other factors including $k_{0,c}, \gamma_{O_2}, \delta_{AFL}, \delta_{CFL}, \delta_{ELE}$ are set as rather sensitive sections while rest of empirical and geometric parameters are regard as insensitive ones. According to the classifications above, the Monte Carlo approach is introduced to assess the reliability of simulation.
4. Sensitivity analysis of single parameters at different locations is presented as the basis for structural optimization along the channel length. For counter flow, highest sensitivity is obtained at the position nearby the channel center duo to the combination effects of temperature and microstructural parameters. Then a non-uniform distribution approach based on SA method is proposed by authors and it is observed that microstructural optimization focused on high sensitivity positions is more efficient than equivalent optimization for all locations.

Acknowledgements

This work is supported by the National Key Research and Development Program of China (2017YFB0601904). M. Ni thanks the funding support (Project Number:

PolyU 152214/17E) from Research Grant Council, University Grants Committee, Hong Kong SAR.

Reference

[1] Jia J, Abudula A, Wei L, et al. Performance comparison of three solid oxide fuel cell power systems. International Journal of Energy Research, 2013, 37(14): 1821-1830.

[2] Ince A C, Karaoglan M U, Glüsen A, et al. Semiempirical thermodynamic modeling of a direct methanol fuel cell system[J]. International Journal of Energy Research, 2019.

[3] Min CH, He YL, Liu XL, et al. Parameter sensitivity examination and discussion of PEM fuel cell simulation model validation: Part II: results of sensitivity analysis and validation of the model. Power Sources 2006;160(1):374–85.

[4] Saltelli, A., Ratto, M., Andres, T., Campolongo, F., Cariboni, J., Gatelli, D., Saisana, M., Tarantola, S., 2008. Global Sensitivity Analysis. The Primer. John Wiley and Sons

[5] Pilkey O H, Pilkey-Jarvis L. Useless arithmetic: why environmental scientists can't predict the future. Columbia University Press, 2007.

[6] Santner T J, Williams B J, Notz W, et al. The design and analysis of computer experiments New York: Springer, 2003.

[7] Oakley J E, O'Hagan A. Probabilistic sensitivity analysis of complex models: a Bayesian approach. Journal of the Royal Statistical Society: Series B (Statistical Methodology), 2004, 66(3): 751-769.

[8] Saltelli A, Annoni P. How to avoid a perfunctory sensitivity analysis. Environ Modell Software 2010;25(12):1508–17

[9] Saltelli A. Sensitivity analysis for importance assessment. Risk Anal 2002;22(3):579–90

[10] Ferretti F, Saltelli A, Tarantola S. Trends in sensitivity analysis practice in the last decade. Science of the Total Environment, 2016, 568: 666-670.

[11] Wagner H M. Global sensitivity analysis. Operations Research, 1995, 43(6):

948-969.

[12] Sobol' IM. On the distribution of points in a cube and the approximate evaluation of integrals. Zhurnal Vychislitel'noi Matematiki i Matematicheskoi Fiziki 1967;7(4):784–802.

[13] Sobol IM. Uniformly distributed sequences with an additional uniform property. USSR Comput Math Math Phys 1976;16(5):236–42.

[14] Sobol IM. Sensitivity estimates for nonlinear mathematical models. Math Modell Comput Exp 1993;1(4):407–14.

[15] Rabitz H, Aliş Ö F, Shorter J, et al. Efficient input—output model representations. Computer Physics Communications, 1999, 117(1-2): 11-20.

[16] Borgonovo E. A new uncertainty importance measure. Reliability Engineering & System Safety, 2007, 92(6): 771-784.

[17] Morris M D. Factorial sampling plans for preliminary computational experiments. Technometrics, 1991, 33(2): 161-174.

[18] Campolongo F, Cariboni J, Saltelli A. An effective screening design for sensitivity analysis of large models. Environmental modelling & software, 2007, 22(10): 1509-1518.

[19] Chan S H, Khor K A, Xia Z T. A complete polarization model of a solid oxide fuel cell and its sensitivity to the change of cell component thickness. Journal of power sources, 2001, 93(1-2): 130-140.

[20] Campanari S, Iora P. Definition and sensitivity analysis of a finite volume SOFC model for a tubular cell geometry. Journal of Power Sources, 2004, 132(1-2): 113-126.

[21] Nagel F P, Schildhauer T J, Biollaz S M A, et al. Charge, mass and heat transfer interactions in solid oxide fuel cells operated with different fuel gases—a sensitivity analysis. Journal of Power Sources, 2008, 184(1): 129-142.

[22] Ni M, Leung M K H, Leung D Y C. Parametric study of solid oxide fuel cell performance. Energy Conversion and Management, 2007, 48(5): 1525-1535.

[23] Vijay P, Tadé M O, Shao Z. Statistical method - based calibration and

validation of a solid oxide fuel cell model. International Journal of Energy Research, 2018.

[24] Campolongo F, Braddock R. Sensitivity analysis of the IMAGE Greenhouse model[J]. Environmental modelling & software, 1999, 14(4): 275-282.

[25] Chevalier S, Josset C, Auvity B. Analytical solutions and dimensional analysis of pseudo 2D current density distribution model in PEM fuel cells. Renewable energy, 2018, 125: 738-746.

[26] Bao C, Shi Y, Croiset E, et al. A multi-level simulation platform of natural gas internal reforming solid oxide fuel cell–gas turbine hybrid generation system: Part I. Solid oxide fuel cell model library. Journal of Power Sources, 2010, 195(15): 4871-4892.

[27] Li C, Shi Y, Cai N. Elementary reaction kinetic model of an anode-supported solid oxide fuel cell fueled with syngas. Journal of power sources, 2010, 195(8): 2266-2282.

[28] Wu C, Yang Z, Huo S, et al. Modeling and optimization of electrode structure design for solid oxide fuel cell. International Journal of Hydrogen Energy, 2018, 43(31): 14648-14664.

[29] Bao C, Jiang Z, Zhang X. Mathematical modeling of synthesis gas fueled electrochemistry and transport including H2/CO co-oxidation and surface diffusion in solid oxide fuel cell. Journal of Power Sources, 2015, 294: 317-332.

[30] Namwong L, Authayanun S , Saebea D , et al. Modeling and optimization of proton-conducting solid oxide electrolysis cell: Conversion of CO2 into value-added products. Journal of Power Sources, 2016, 331:515-526.

[31] Wang B, Deng H, Jiao K. Purge strategy optimization of proton exchange membrane fuel cell with anode recirculation. Applied energy, 2018, 225: 1-13.

[32] Chen D, Lin Z, Zhu H, et al. Percolation theory to predict effective properties of solid oxide fuel-cell composite electrodes. Journal of Power Sources, 2009; 191(2):240-252.

[33] Zhang Y, Xia C. Film percolation for composite electrodes of solid oxide fuel cells. Electrochimica Acta, 2011, 56(13):4763-4769.

[34] Shi Y, Cai N, Li C, et al. Modeling of an anode-supported Ni–YSZ| Ni–ScSZ| ScSZ| LSM–ScSZ multiple layers SOFC cell: Part I. experiments, model development and validation. Journal of Power Sources, 2007, 172(1): 235-245.

[35] Beale S B, Reimer U, Froning D, et al. Stability issues of fuel cell models in the activation and concentration regimes. Journal of Electrochemical Energy Conversion and Storage, 2018, 15(4): 041008.

[36] Jiang Y, Yang Z, Jiao K, et al. Sensitivity analysis of uncertain parameters based on an improved proton exchange membrane fuel cell analytical model. Energy Conversion and Management, 2018, 164: 639-654.

[37] Wang Z, Zhang N, Qiao J, et al. Improved SOFC performance with continuously graded anode functional layer. Electrochemistry Communications, 2009, 11(6): 1120-1123.

[38] Bao C, Wang Y, Feng D, et al. Macroscopic modeling of solid oxide fuel cell (SOFC) and model-based control of SOFC and gas turbine hybrid system. Progress in Energy and Combustion Science, 2018, 66: 83-140.

[39] Lee S, Kim H, Yoon K J, et al. The effect of fuel utilization on heat and mass transfer within solid oxide fuel cells examined by three-dimensional numerical simulations International Journal of Heat and Mass Transfer, 2016, 97: 77-93.

Figure and Table caption

Figure 1 Illustration of anode-supported solid oxide fuel cell structure.

Figure 2 Comparison between modelling prediction and experiments data [34]. (a) current density - voltage curves; (b) Overpotential.

Figure 3 Feasibility assessment of elementary effects by two sample Kolmogorov-Smirnov (K-S) test. (a) Comparison between standard result 1 and selected result 2; (b) Comparison between standard result 1 and selected result 3.

Figure 4 Simulation results for three selected cases.

Figure 5 Sensitivity characteristics of structural parameters of anode/cathode function layers. (a)&(b), Geometric parameters at FL, 1500 A m^{-2}; (c)&(d), Geometric parameters at FL, 7500 A m^{-2}.

Figure 6 Influence of current density variation on parametric sensitivity. (a) Thickness; (b) Electronic conducting particle radius; (c) Relative volume fraction of electronic conducting materials. (d) Particle radii ratio.

Figure 7 Sensitivity characteristics for rest of geometric parameters and electrochemical parameters; (a)&(b), Geometric parameters at all zones, 1500 A m^{-2}; (c)&(d), Geometric parameters at all zones, 7500 A m^{-2}; (e)&(f), Electrochemical parameters, 1500 A m^{-2}; (g)&(h), Electrochemical parameters, 7500 A m^{-2}.

Figure 8 Influence of current density variation on parametric sensitivity. (a) Thickness of electrolyte and porosity; (b) Reaction order of O_2 and pre-exponential factor.

Figure 9 Histograms of sensitivity distribution for all input parameters, 1500 A m^2

Figure 10 Scatterplots for comparison of output voltage owing to sensitive factors, insensitive factors and all factors. (a) Comparison between insensitive factors and all factors; (b) Comparison between sensitive factors and all factors.

Figure 11 Sensitivity distribution of single parameters along the channel direction. (a) Particle radius; (b) Porosity; (c) Relative volume fraction; (d) Particle radii ratios.

Figure 12 Non-uniform distribution of microstructural factors along the channel direction. (a) Uneven distribution strategy of microscopic parameters along the channel length; (b) Effects of uniform and non-uniform microstructure distribution on cell performance.

Table 1 Cell structures and basic operation conditions [26 - 29].

Table 2 Source terms.

Table 3. Diffusion coefficients [30].

Table 4 Three selected groups of parameters.

Table 5 Parametric ranges for global sensitivity analysis.

Table 6 Sensitive degree of 24 parameters.

Table 7 Non-uniform distribution of microscopic structure along the channel length.

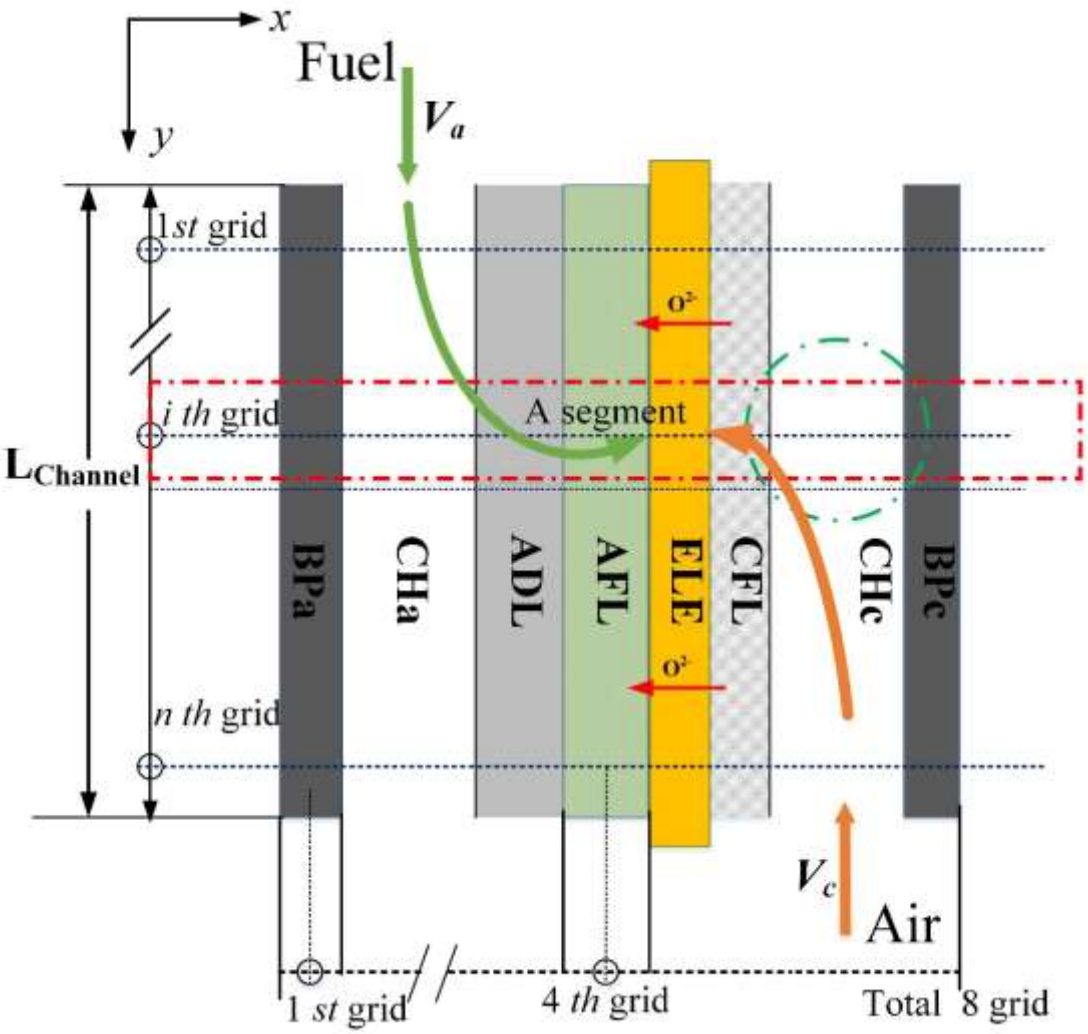

Figure 1 Illustration of anode-supported solid oxide fuel cell structure.

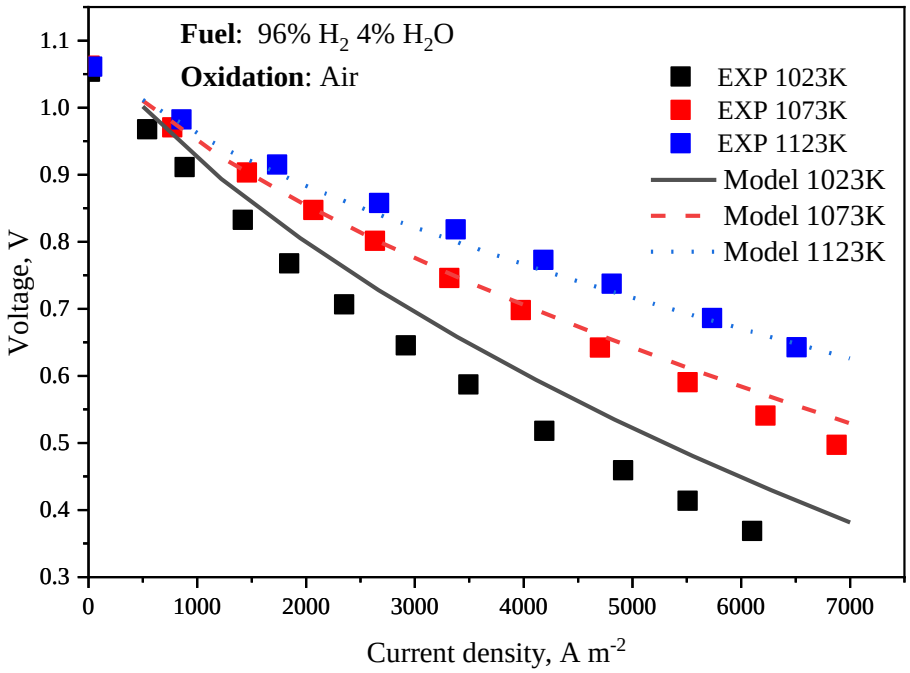

(a)

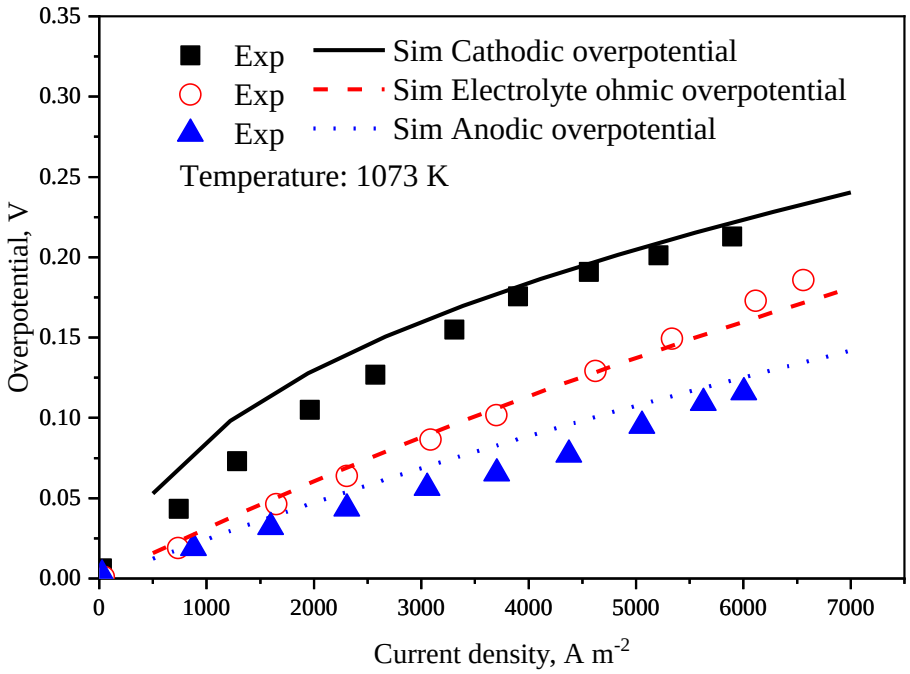

(b)

Figure 2 Comparison between modelling prediction and experiments data [34]. (a) current density - voltage curves; (b) Overpotential.

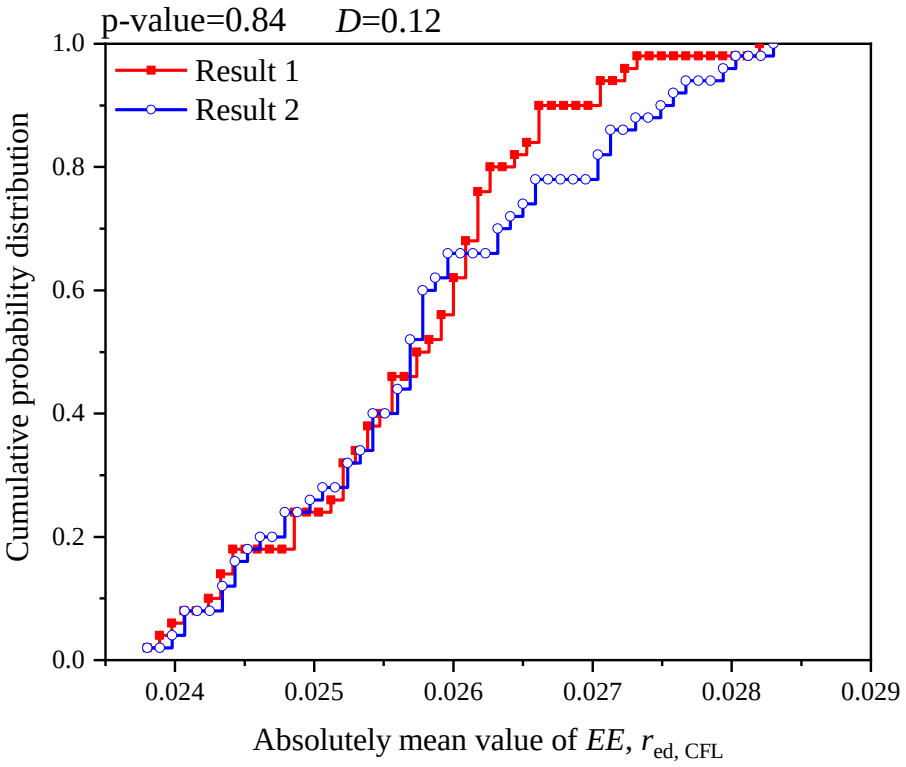

(a)

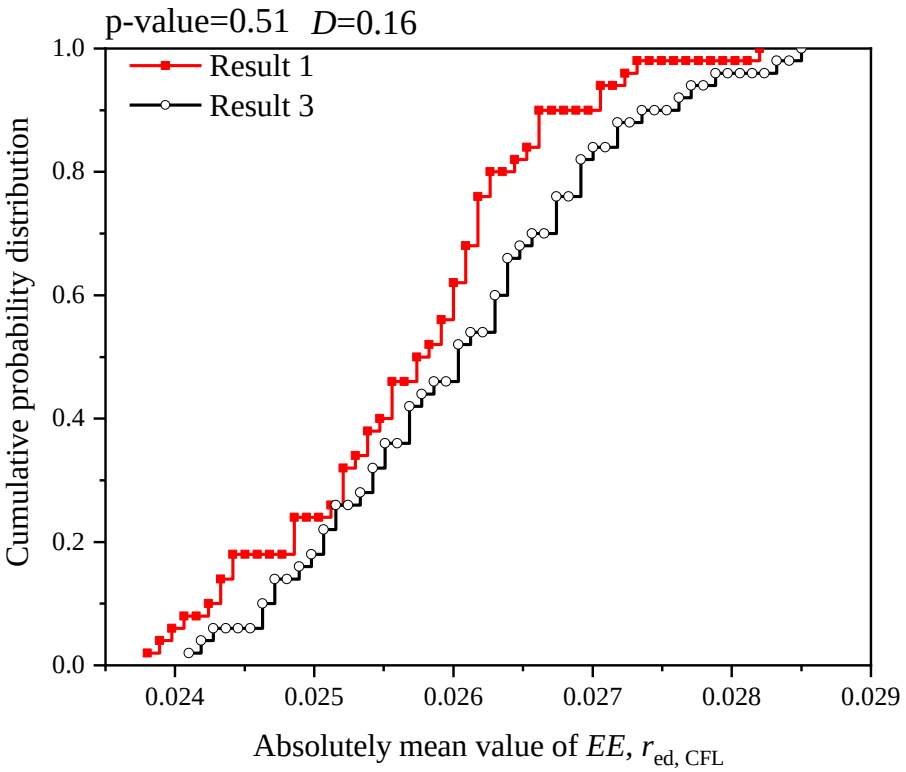

(b)

Figure 3 Feasibility assessment of elementary effects by two sample Kolmogorov-Smirnov (K-S) test. (a) Comparison between standard result 1 and selected result 2; (b) Comparison between standard result 1 and selected result 3.

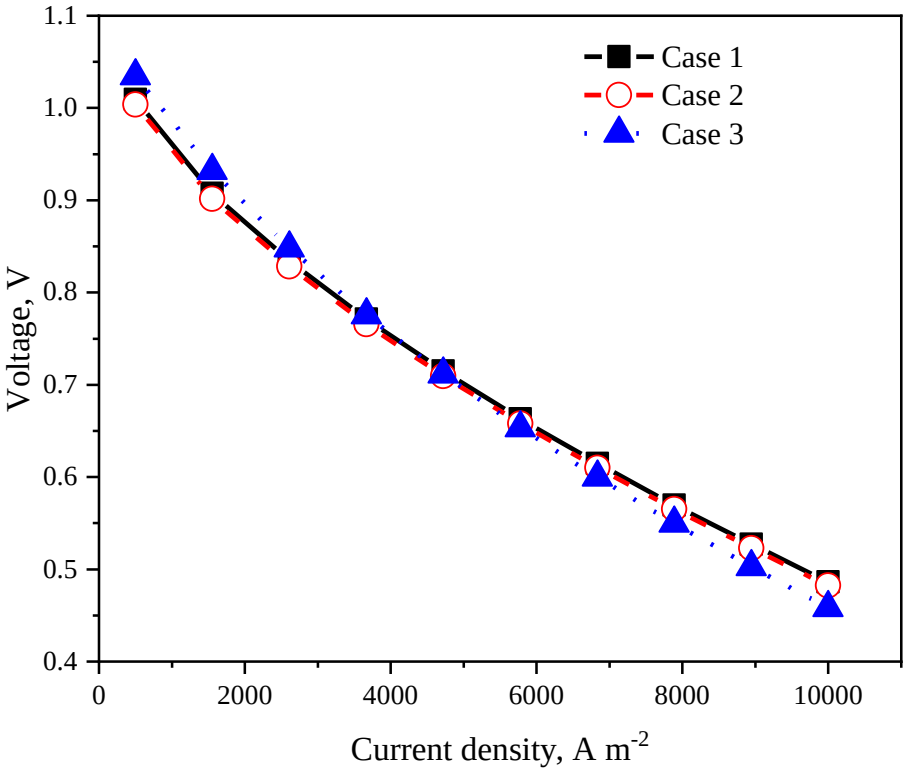

Figure 4 Simulation results for three selected cases.

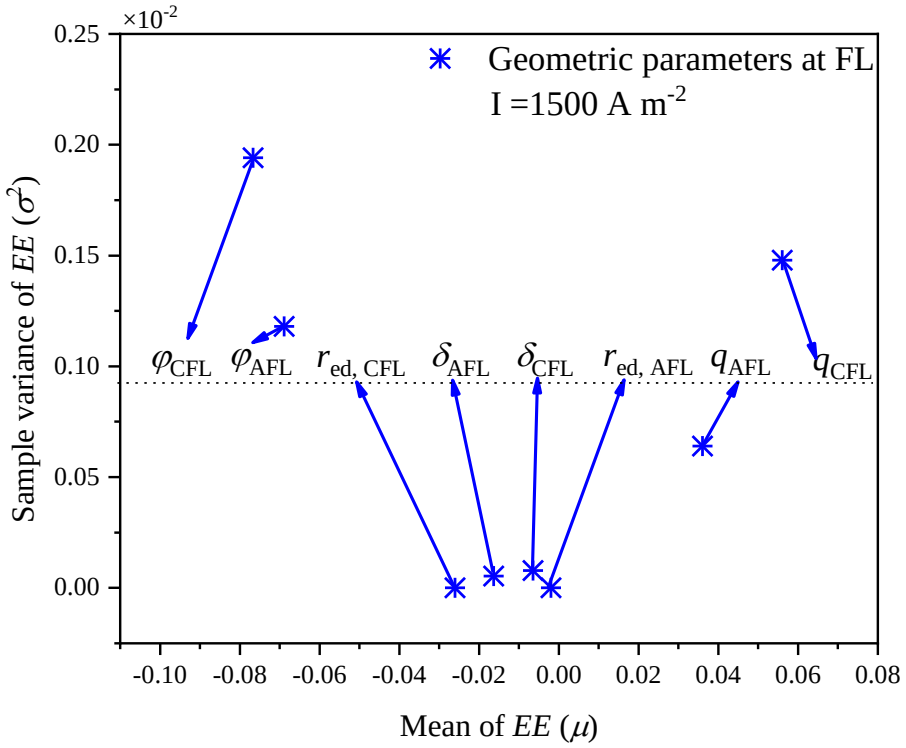
×10-2
0.25
0.20
0.15
0.10
0.05
0.00
Sample variance of EE (σ2)
Geometric parameters at FL
I =1500 A m-2
φCFL
φAFL
red, CFL
δAFL
δCFL
red, AFL
qAFL
qCFL
-0.10
-0.08
-0.06
-0.04
-0.02
0.00
0.02
0.04
0.06
0.08
Mean of EE (μ)

(a)

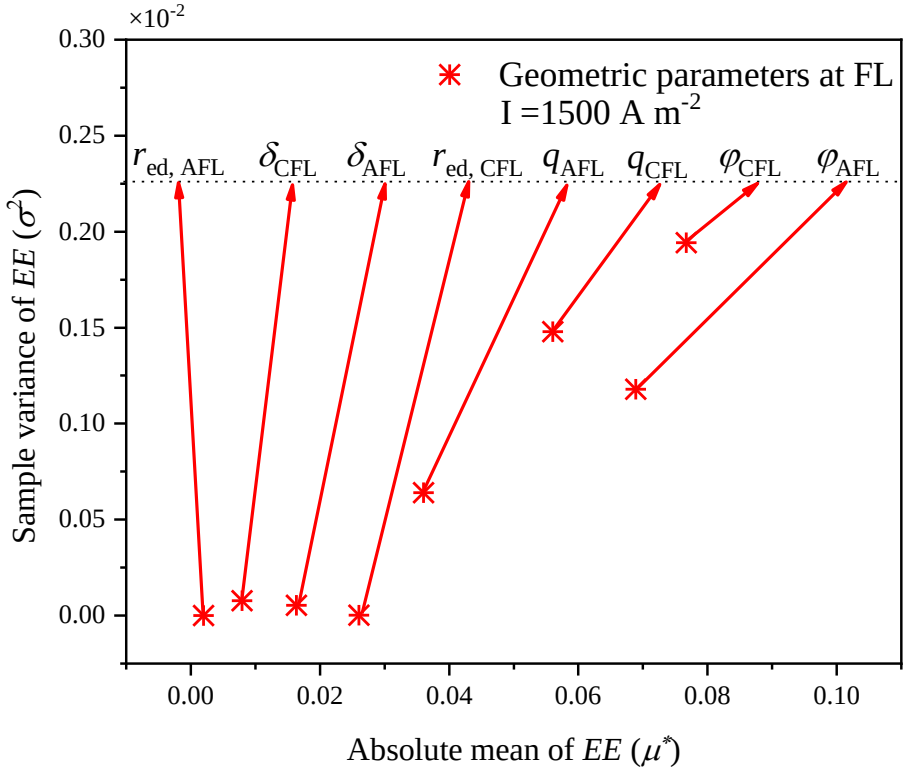
×10-2
0.30
0.25
0.20
0.15
0.10
0.05
0.00
Sample variance of EE (σ2)
Geometric parameters at FL
I =1500 A m-2
red, AFL
δCFL
δAFL
red, CFL
qAFL
qCFL
φCFL
φAFL
0.00
0.02
0.04
0.06
0.08
0.10
Absolute mean of EE (μ*)

(b)

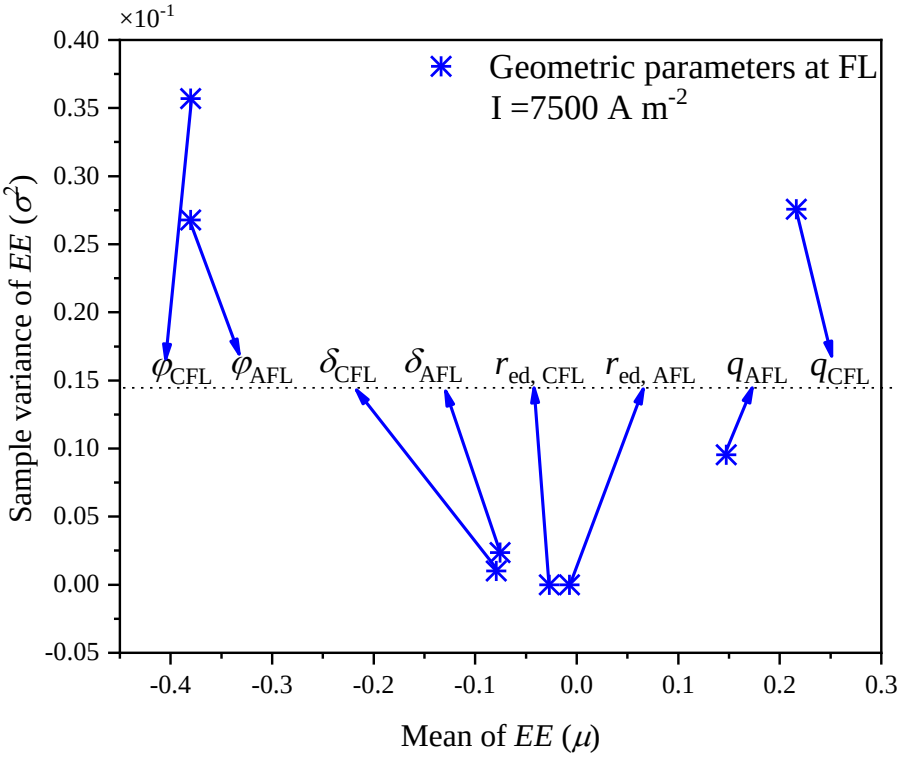

(c)

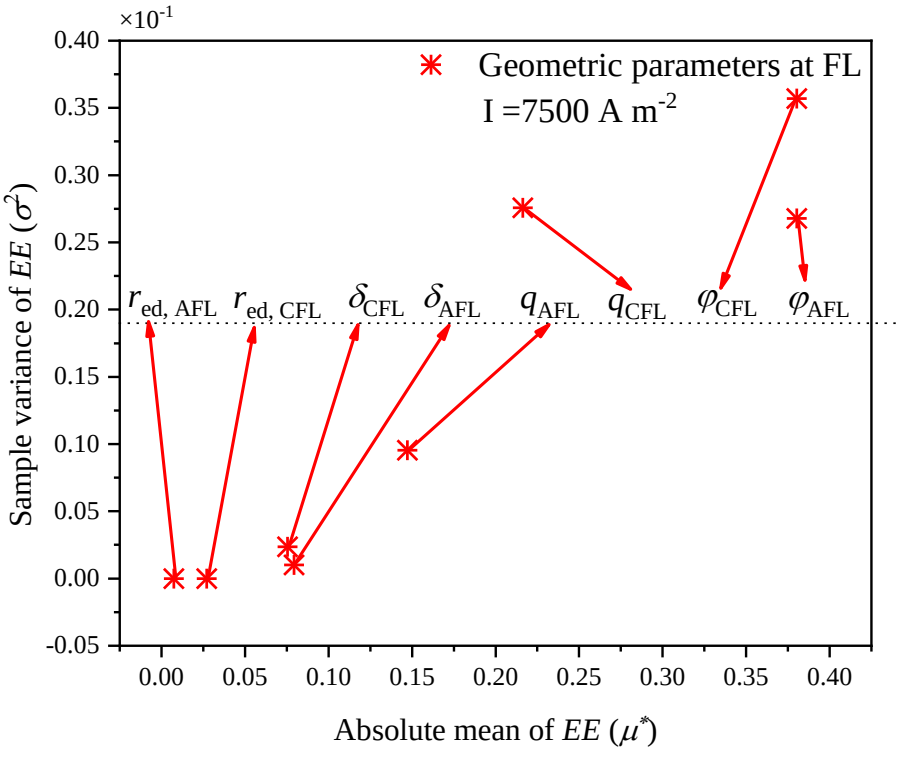

(d)

Figure 5 Sensitivity characteristics of structural parameters of anode/cathode function layers. (a)&(b), Geometric parameters at FL, 1500 A m^{-2}; (c)&(d), Geometric parameters at FL, 7500 A m^{-2}.

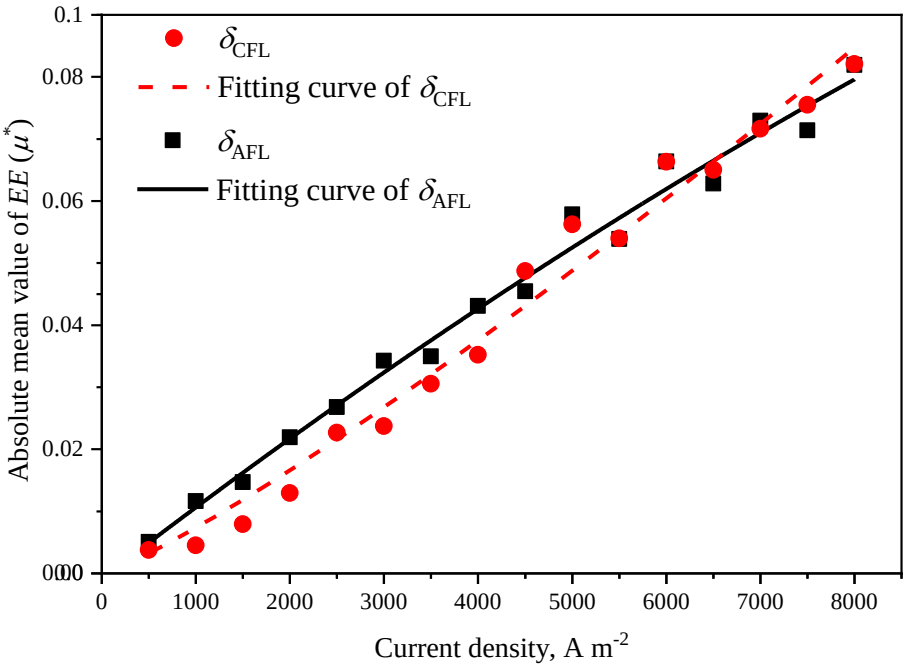
0.1
0.08
0.06
0.04
0.02
0.00
0
1000
2000
3000
4000
5000
6000
7000
8000
Absolute mean value of EE (μ^*)
Current density, A m^{-2}
δ_{CFL}
Fitting curve of δ_{CFL}
δ_{AFL}
Fitting curve of δ_{AFL}

(a)

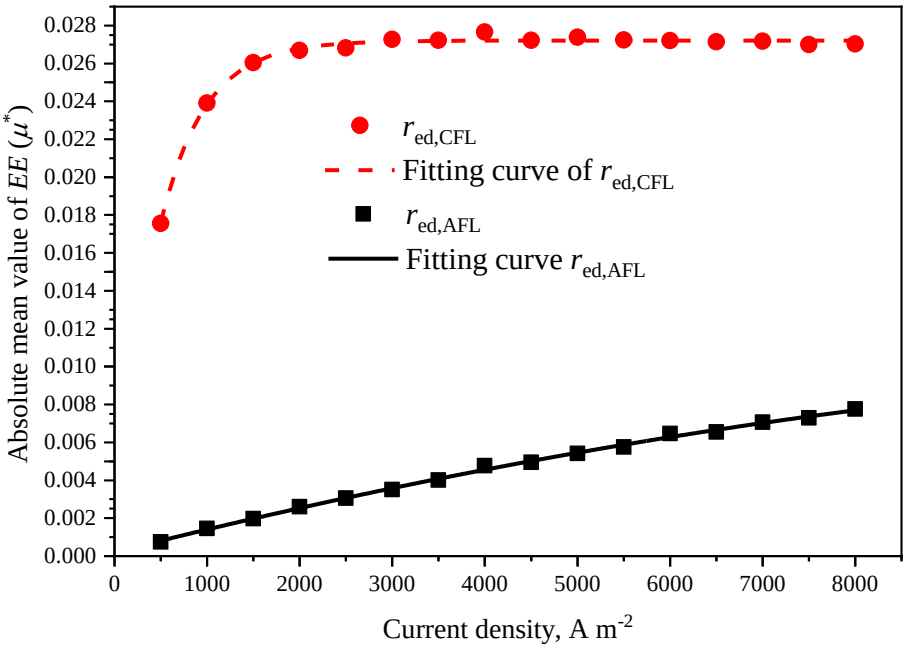
0.028
0.026
0.024
0.022
0.020
0.018
0.016
0.014
0.012
0.010
0.008
0.006
0.004
0.002
0.000
0
1000
2000
3000
4000
5000
6000
7000
8000
Absolute mean value of EE (μ^*)
Current density, A m^{-2}
$r_{ed,CFL}$
Fitting curve of $r_{ed,CFL}$
$r_{ed,AFL}$
Fitting curve $r_{ed,AFL}$

(b)

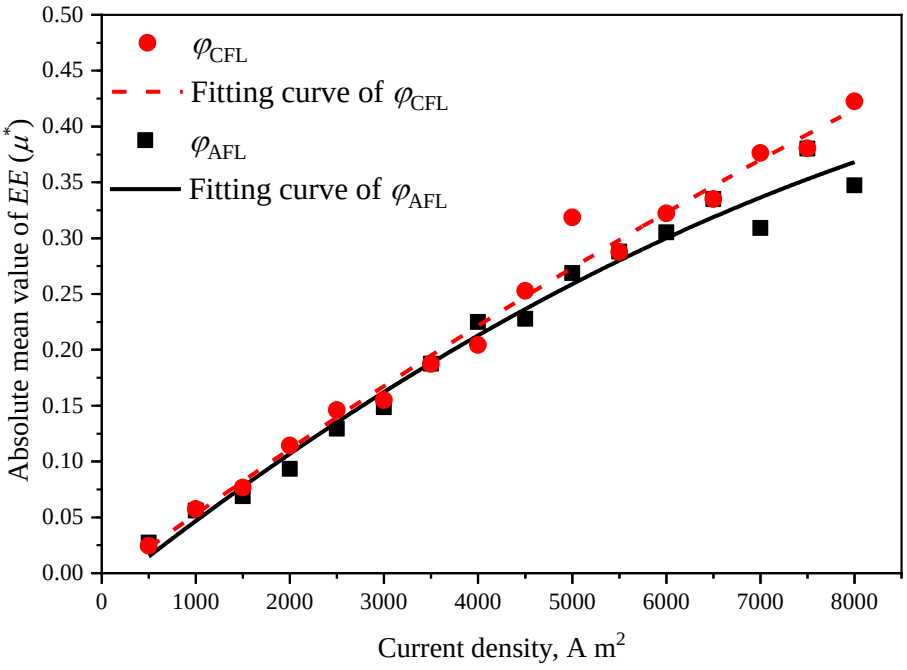

(c)

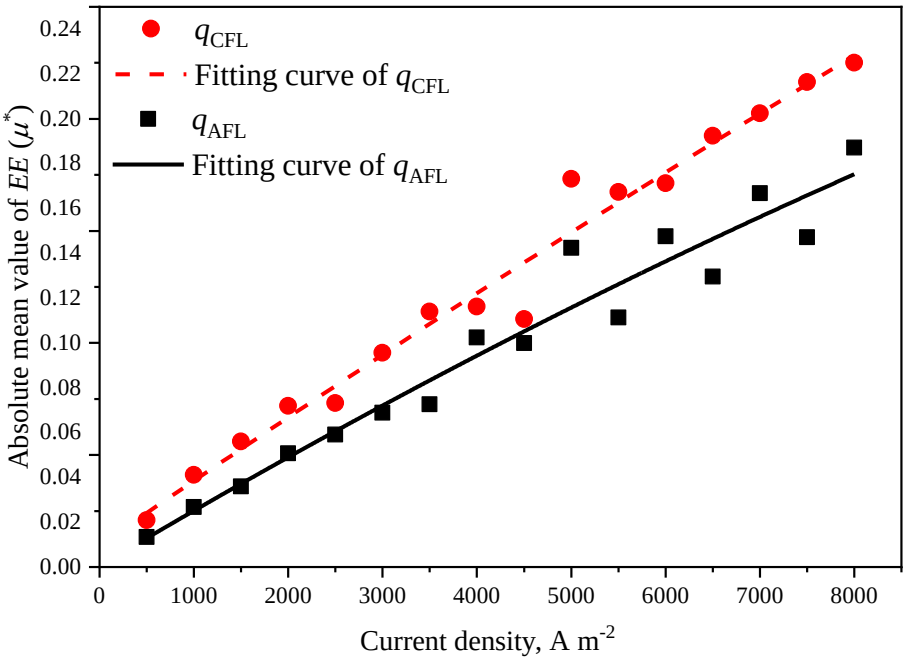

(d)

Figure 6 Influence of current density variation on parametric sensitivity. (a) Thickness; (b) Electronic conducting particle radius; (c) Relative volume fraction of electronic conducting materials. (d) Particle radii ratio.

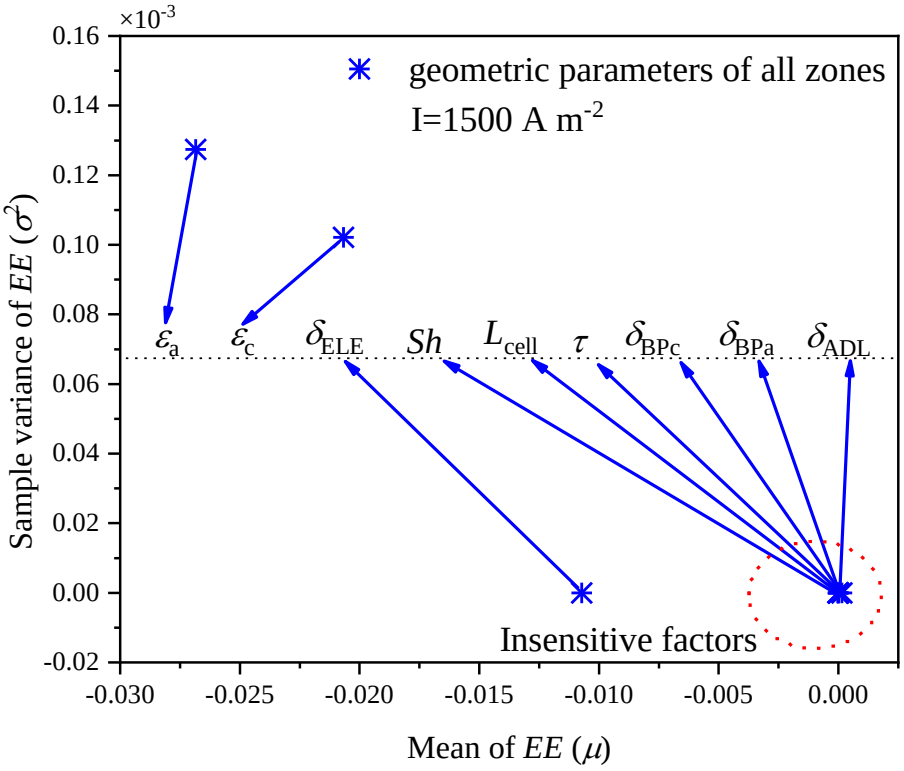
×10-3
0.16
0.14
0.12
0.10
0.08
0.06
0.04
0.02
0.00
-0.02
Sample variance of EE (σ2)
geometric parameters of all zones
I=1500 A m-2
εa
εc
δELE
Sh
Lcell
τ
δBPc
δBPa
δADL
Insensitive factors
-0.030
-0.025
-0.020
-0.015
-0.010
-0.005
0.000
Mean of EE (μ)

(a)

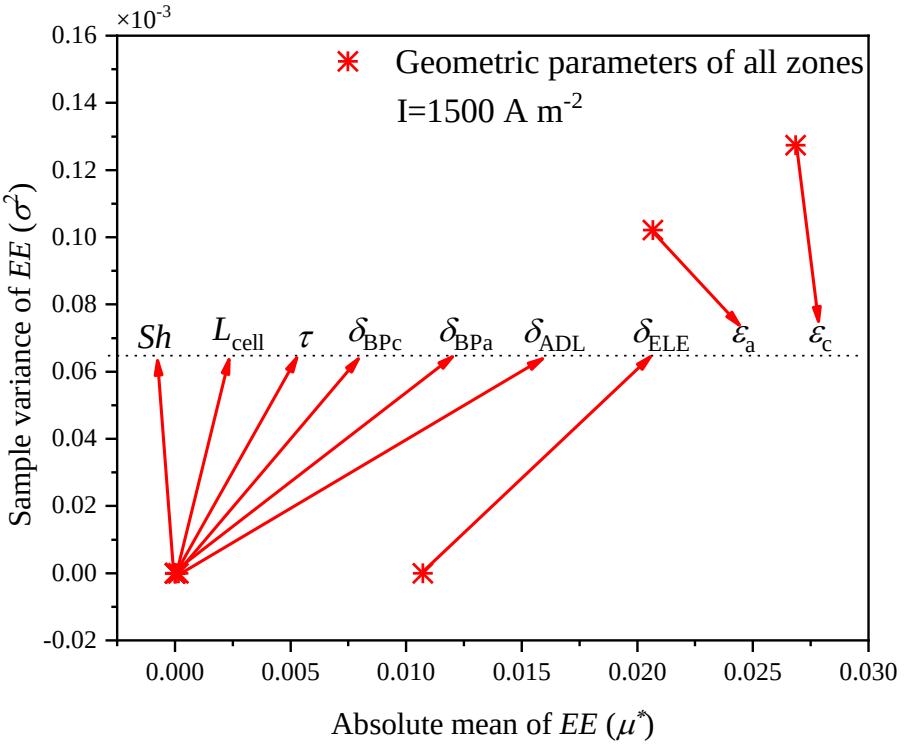
×10-3
0.16
0.14
0.12
0.10
0.08
0.06
0.04
0.02
0.00
-0.02
Sample variance of EE (σ2)
Geometric parameters of all zones
I=1500 A m-2
Sh
Lcell
τ
δBPc
δBPa
δADL
δELE
εa
εc
0.000
0.005
0.010
0.015
0.020
0.025
0.030
Absolute mean of EE (μ*)

(b)

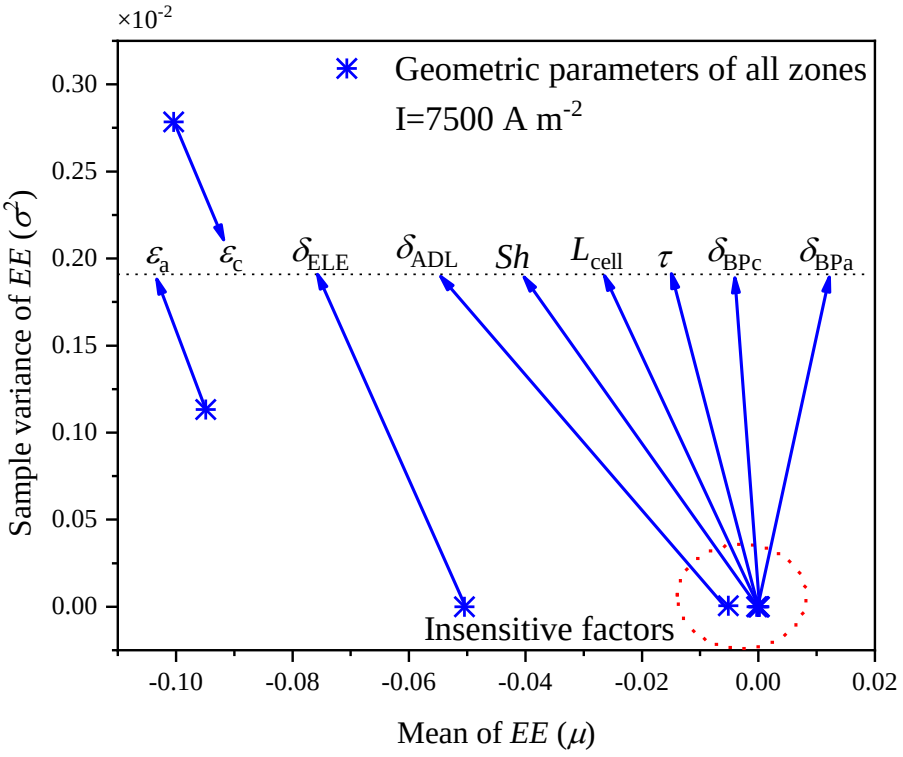
×10-2
Geometric parameters of all zones
I=7500 A m-2
Sample variance of EE (σ2)
εa
εc
δELE
δADL
Sh
Lcell
τ
δBPc
δBPa
Insensitive factors
0.30
0.25
0.20
0.15
0.10
0.05
0.00
-0.10
-0.08
-0.06
-0.04
-0.02
0.00
0.02
Mean of EE (μ)

(c)

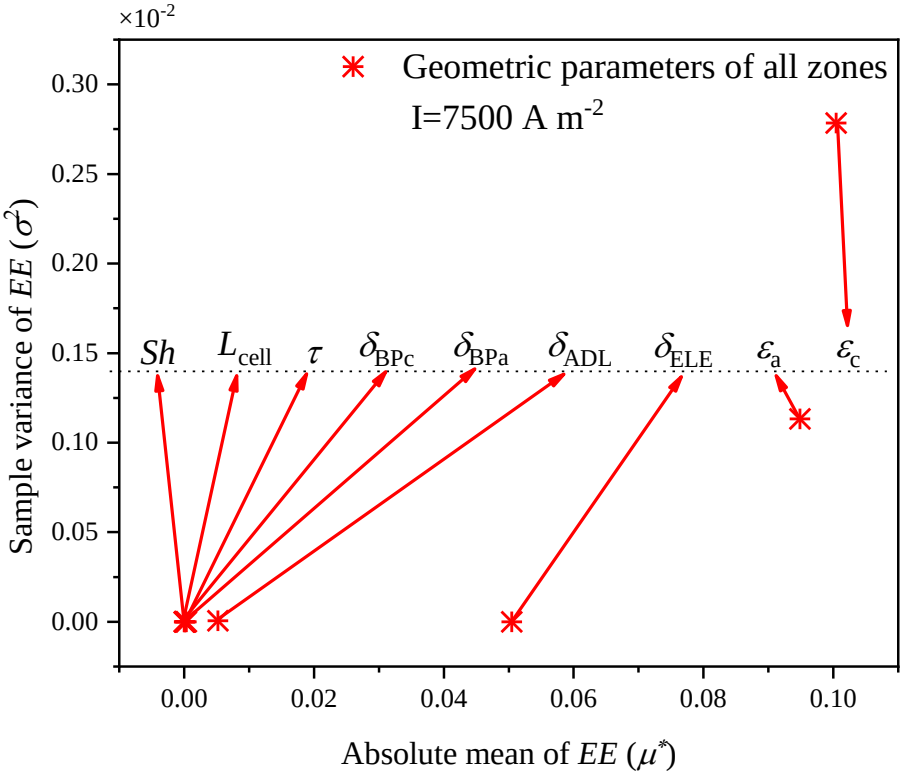
×10-2
Geometric parameters of all zones
I=7500 A m-2
Sample variance of EE (σ2)
Sh
Lcell
τ
δBPc
δBPa
δADL
δELE
εa
εc
0.30
0.25
0.20
0.15
0.10
0.05
0.00
0.00
0.02
0.04
0.06
0.08
0.10
Absolute mean of EE (μ*)

(d)

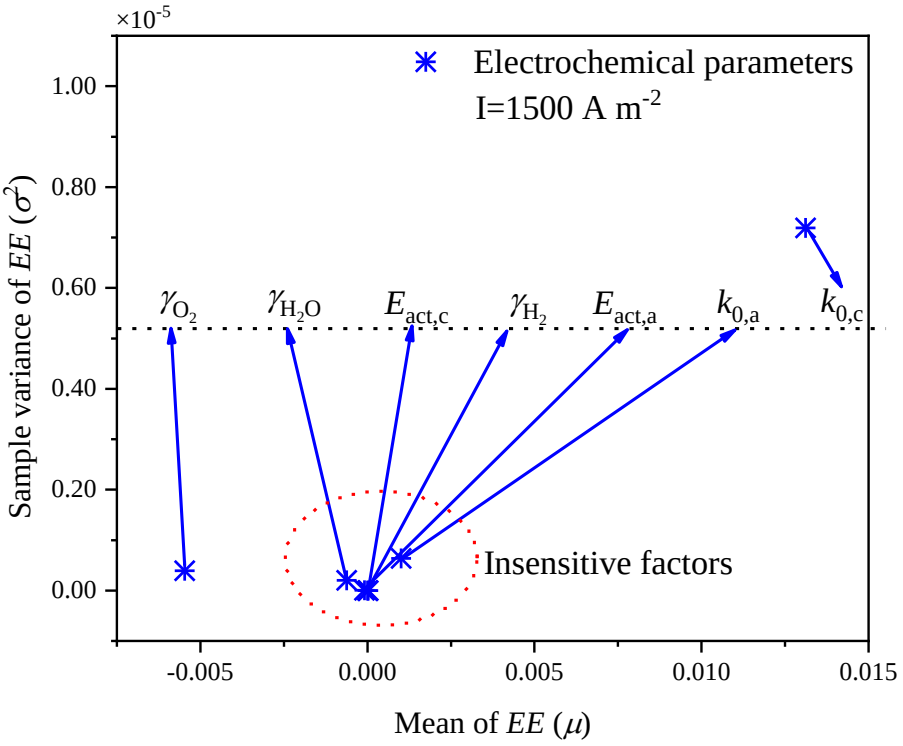
×10-5
Electrochemical parameters
I=1500 A m-2
Sample variance of EE (σ2)
Mean of EE (μ)
γO2
γH2O
Eact,c
γH2
Eact,a
k0,a
k0,c
Insensitive factors
1.00
0.80
0.60
0.40
0.20
0.00
-0.005
0.000
0.005
0.010
0.015

(e)

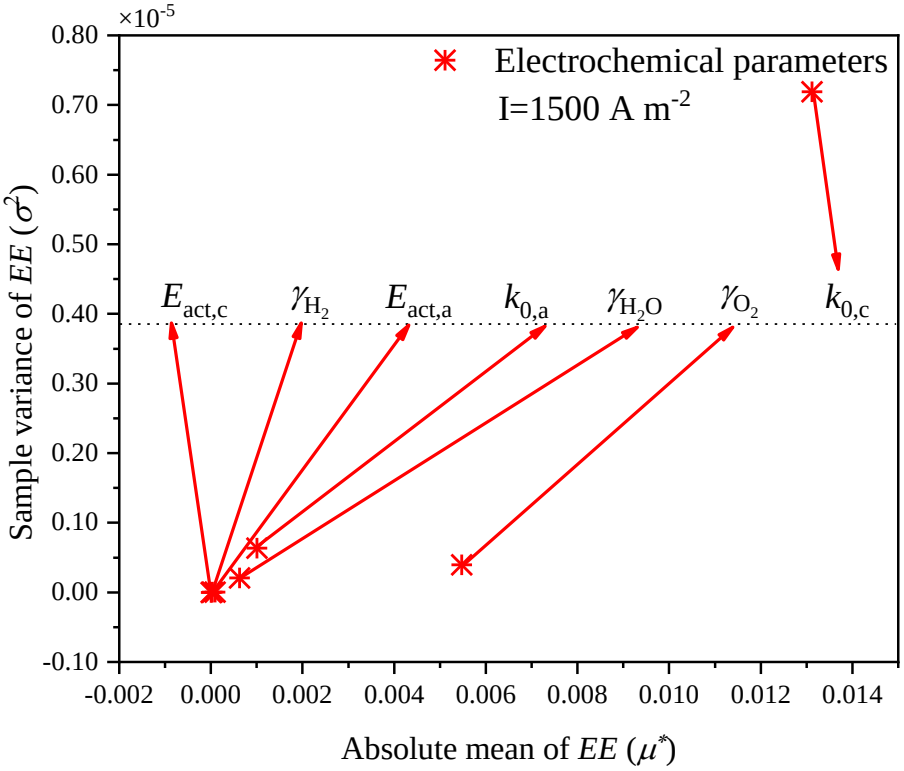
×10-5
Electrochemical parameters
I=1500 A m-2
Sample variance of EE (σ2)
Absolute mean of EE (μ*)
Eact,c
γH2
Eact,a
k0,a
γH2O
γO2
k0,c
0.80
0.70
0.60
0.50
0.40
0.30
0.20
0.10
0.00
-0.10
-0.002
0.000
0.002
0.004
0.006
0.008
0.010
0.012
0.014

(f)

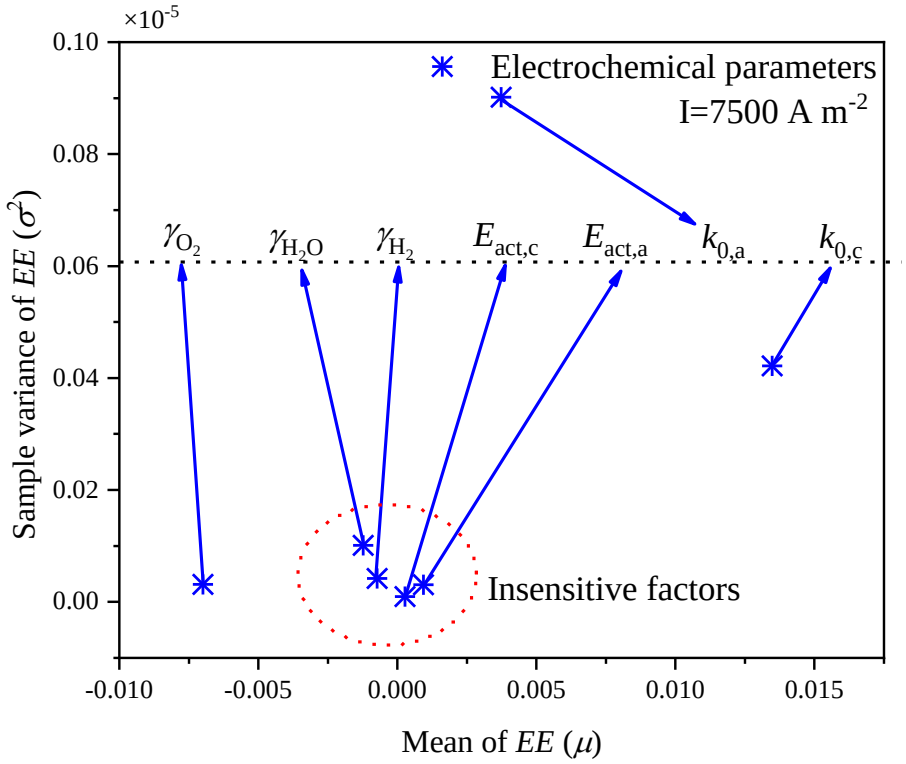

(g)

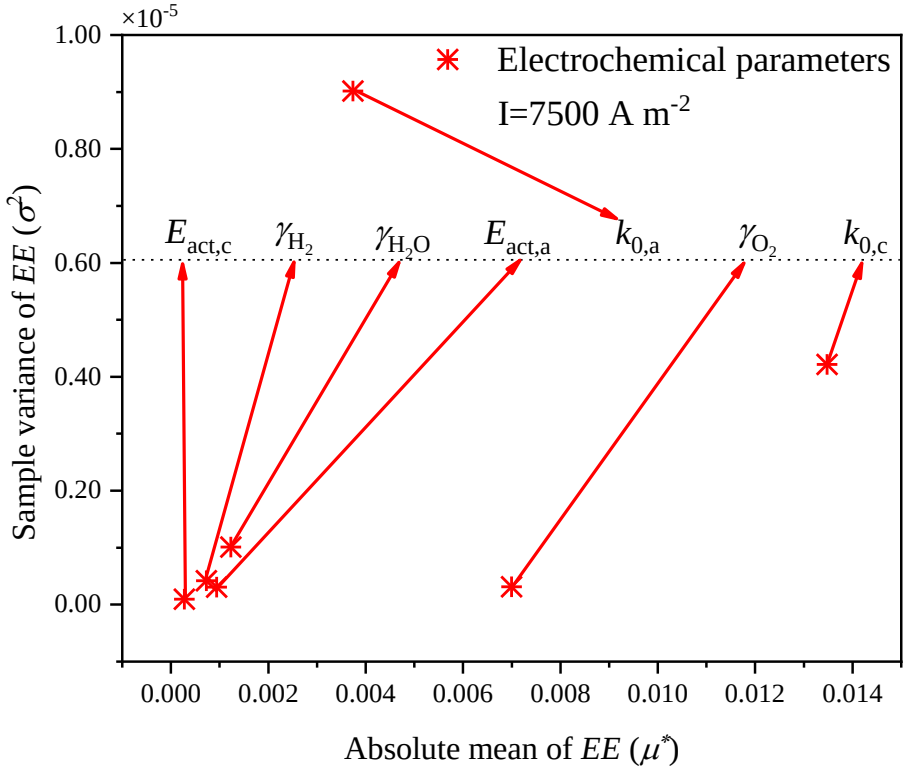

(h)

Figure 7 Sensitivity characteristics for rest of geometric parameters and electrochemical parameters; (a)&(b), Geometric parameters at all zones, 1500 A m^{-2}; (c)&(d), Geometric parameters at all zones, 7500 A m^{-2}; (e)&(f), Electrochemical

parameters, 1500 A m^{-2}; (g)&(h), Electrochemical parameters, 7500 A m^{-2}.

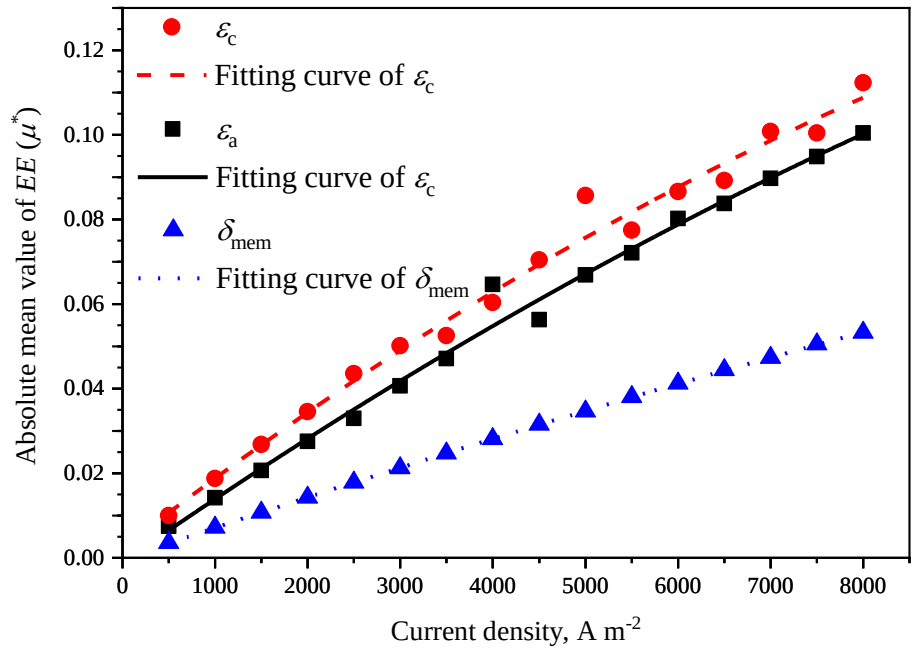

(a)

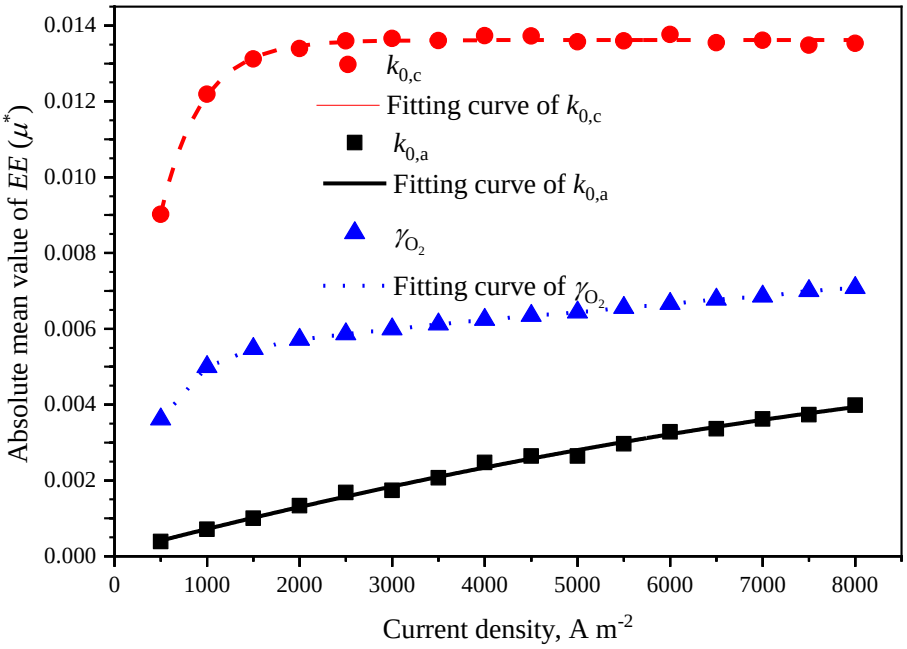

(b)

Figure 8 Influence of current density variation on parametric sensitivity. (a) Thickness of electrolyte and porosity; (b) Reaction order of O_2 and pre-exponential factor.

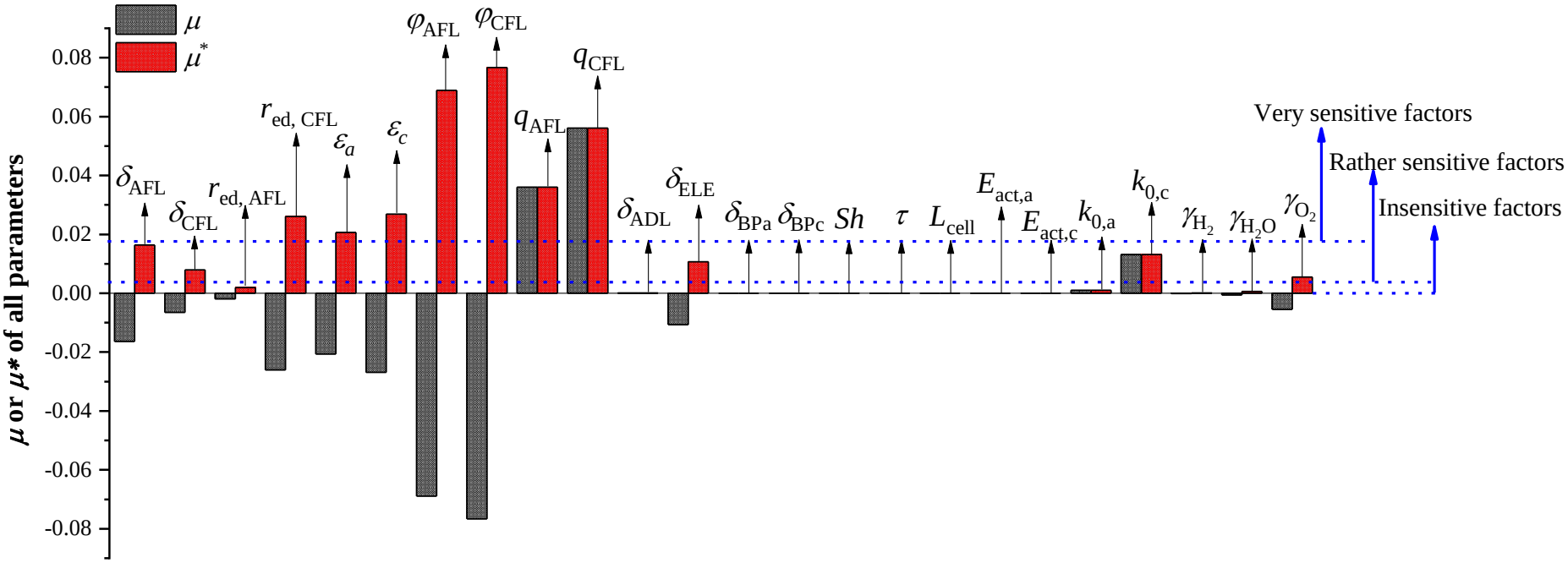

Figure 9 Histograms of sensitivity distribution for all input parameters, 1500 A m^2.

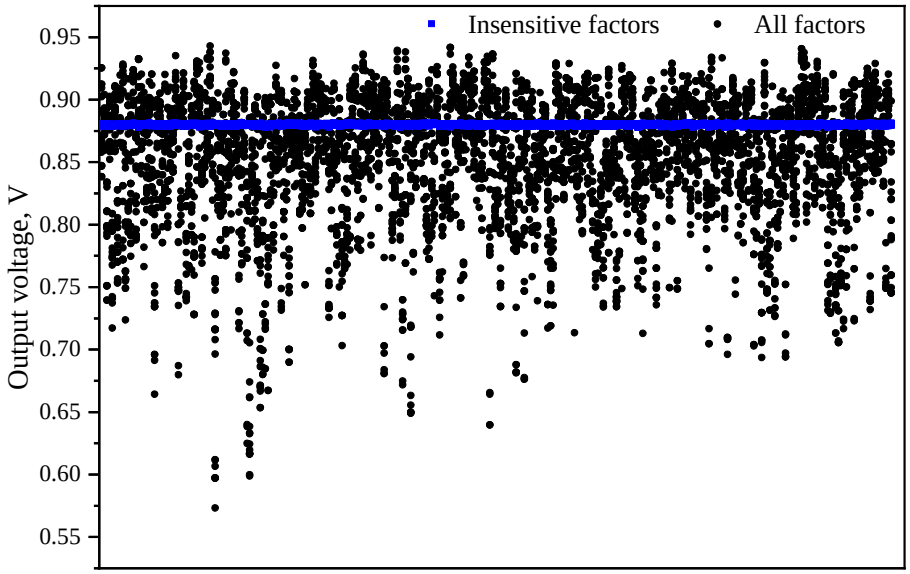

(a)

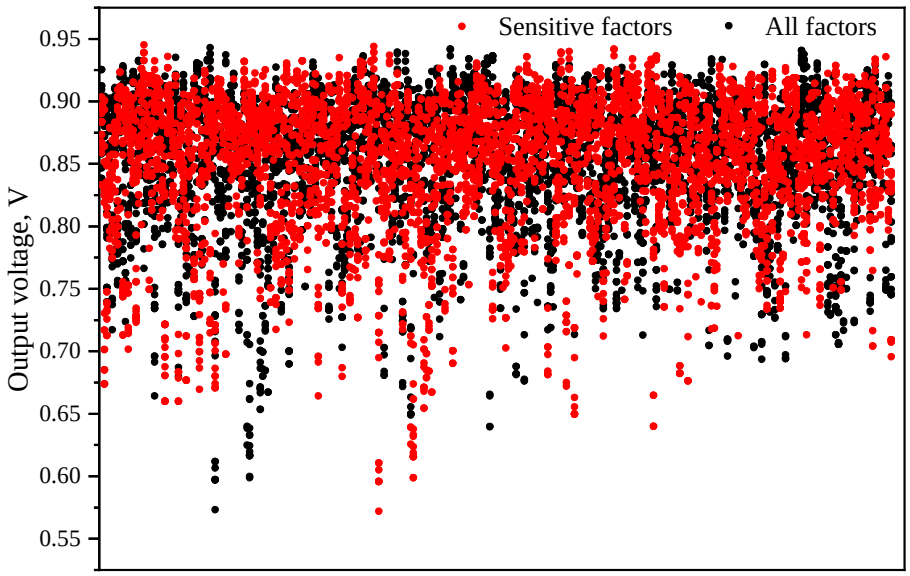

(b)

Figure 10 Scatterplots for comparison of output voltage distribution owing to sensitive factors, insensitive factors and all factors. (a) Comparison between insensitive factors and all factors; (b) Comparison between sensitive factors and all factors.

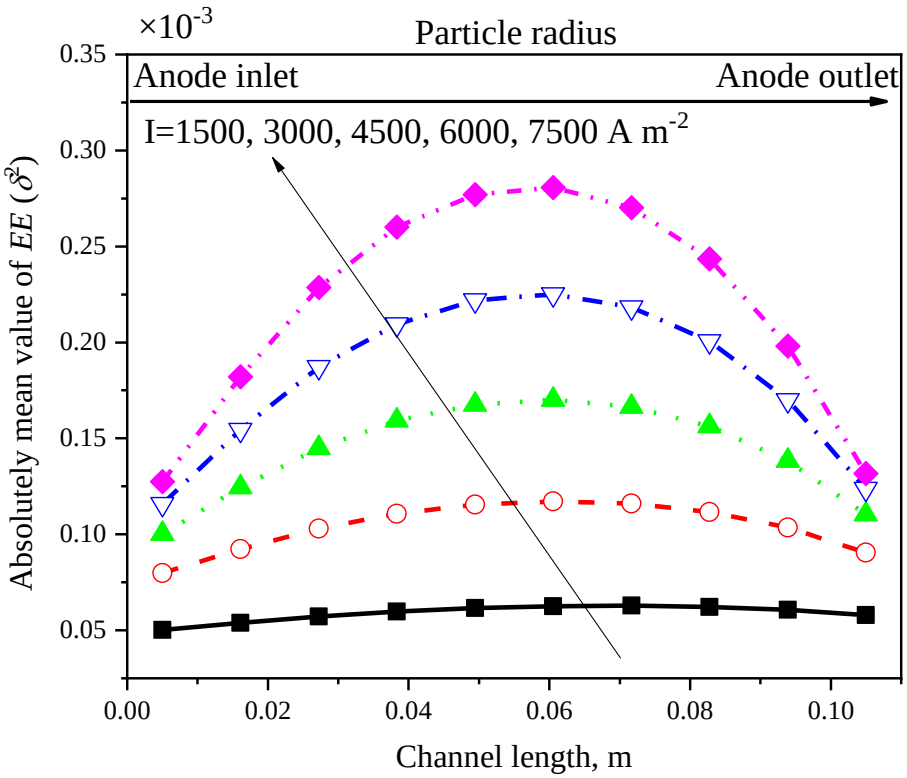
×10-3
Particle radius
Anode inlet
Anode outlet
I=1500, 3000, 4500, 6000, 7500 A m-2
Absolutely mean value of EE (δ2)
0.35
0.30
0.25
0.20
0.15
0.10
0.05
0.00
0.02
0.04
0.06
0.08
0.10
Channel length, m

(a)

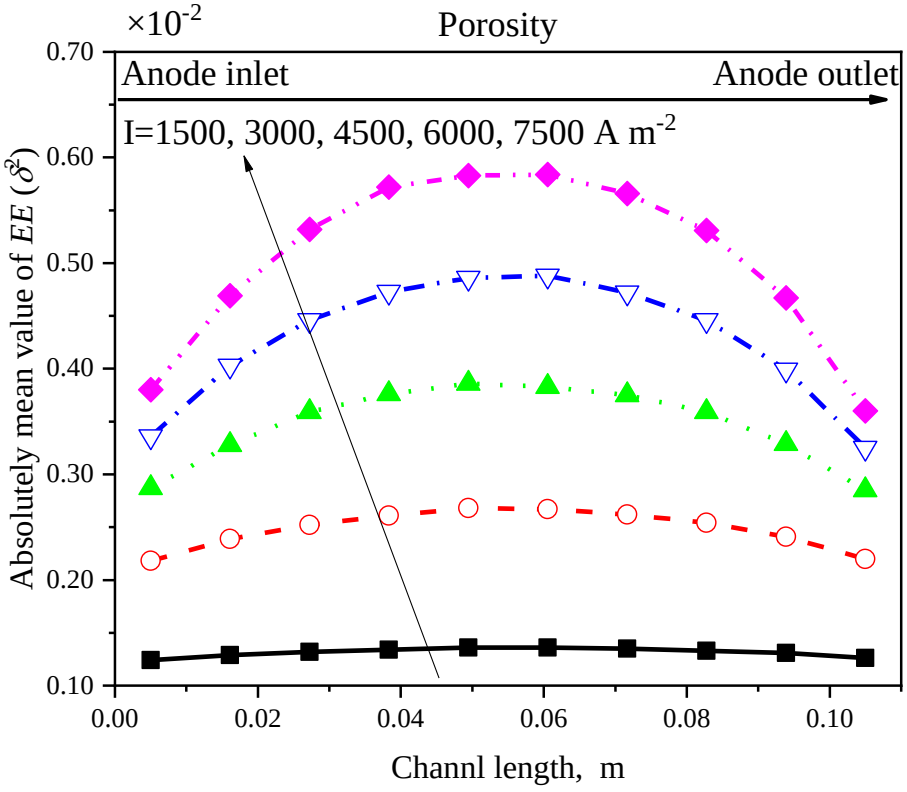
×10-2
Porosity
Anode inlet
Anode outlet
I=1500, 3000, 4500, 6000, 7500 A m-2
Absolutely mean value of EE (δ2)
0.70
0.60
0.50
0.40
0.30
0.20
0.10
0.00
0.02
0.04
0.06
0.08
0.10
Channl length, m

(b)

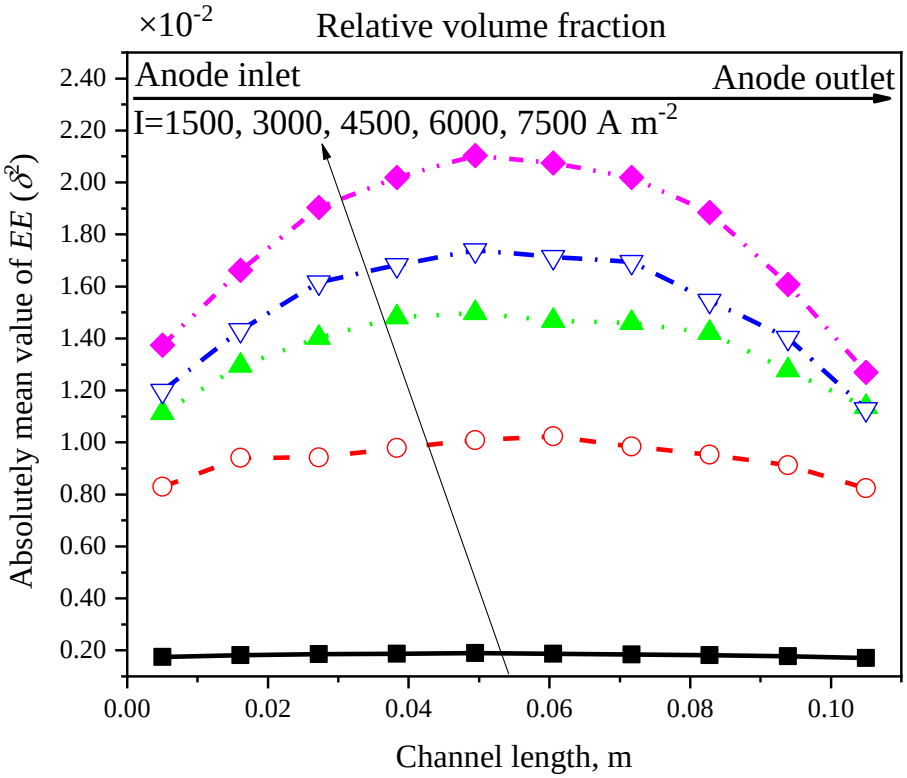

(c)

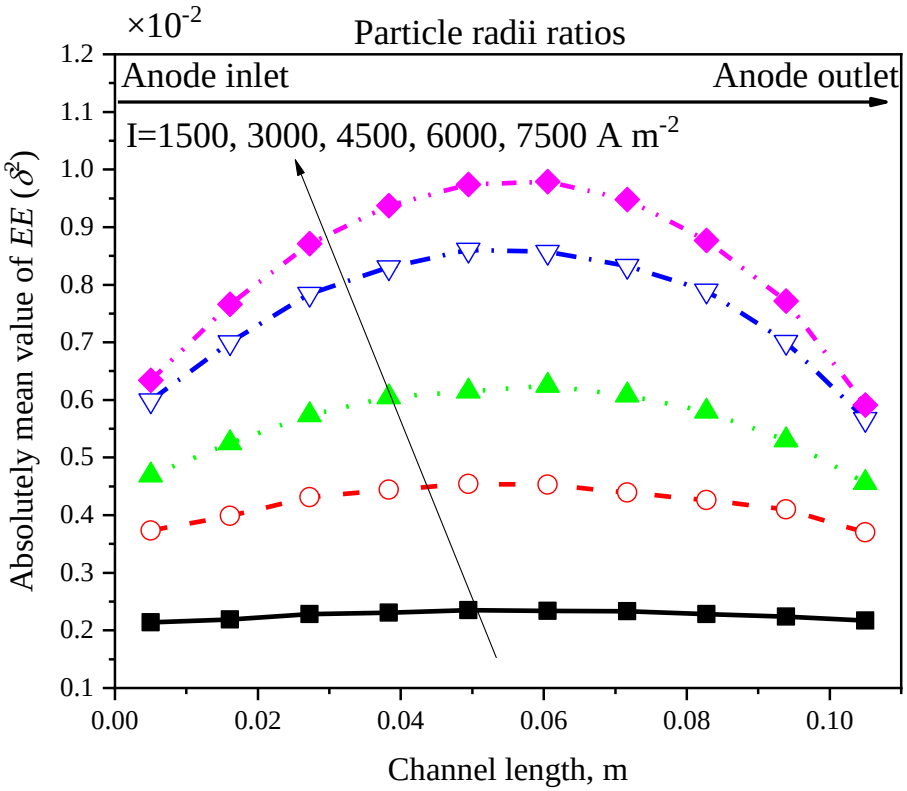

(d)

Figure 11 Sensitivity distribution of single parameters along the channel direction. (a) Particle radius; (b) Porosity; (c) Relative volume fraction; (d) Particle radii ratio.

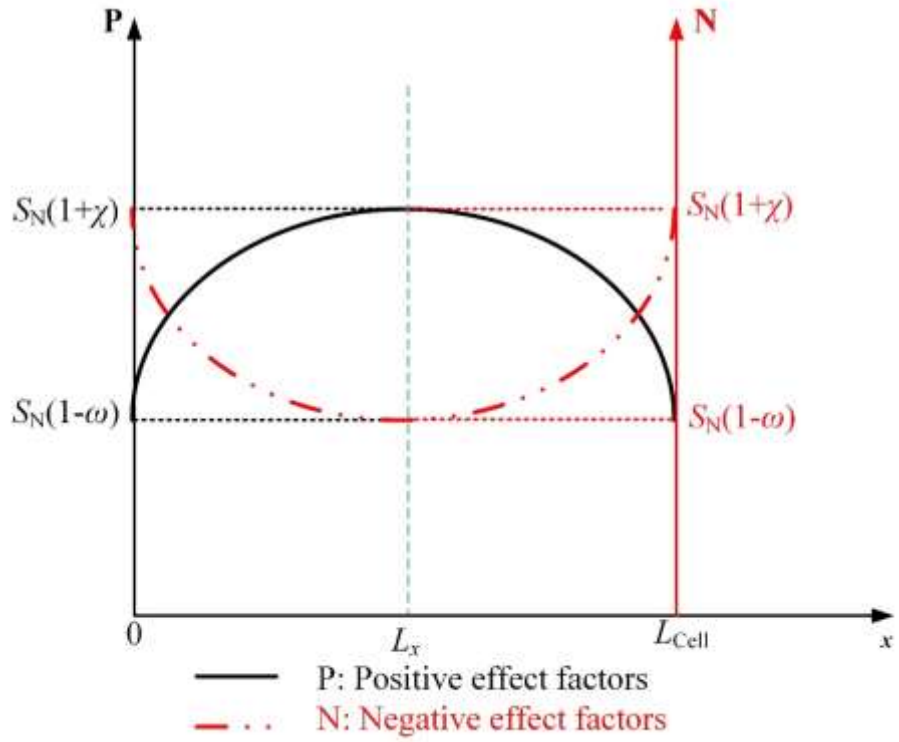

(a)

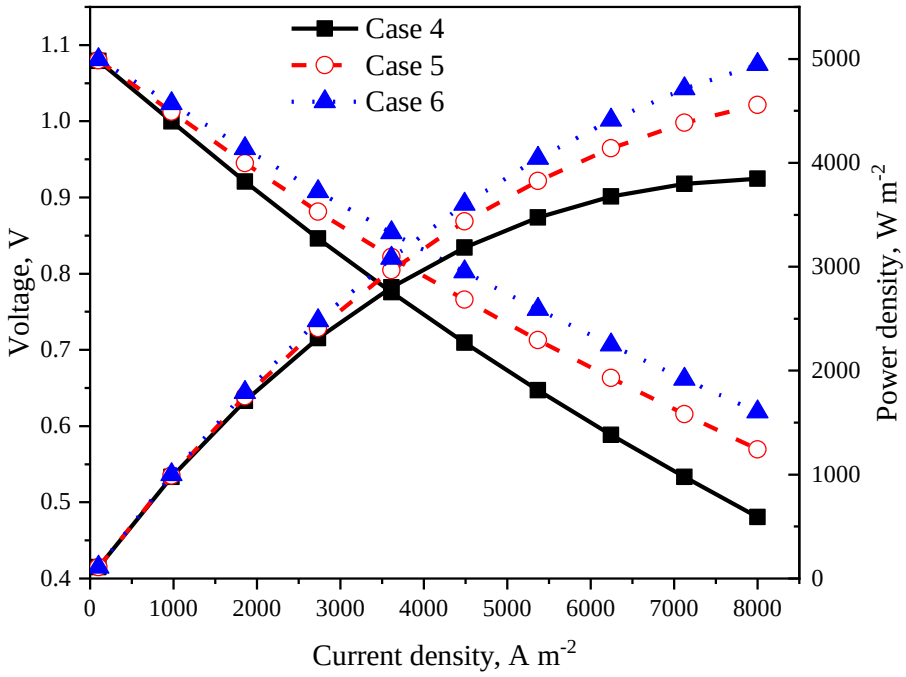

(b)

Figure 12 Non-uniform distribution of microstructural factors along the channel direction. (a) Uneven distribution strategy of microscopic parameters along the channel length; (b) Effects of uniform and non-uniform microstructure distribution on cell performance.

Table 1 Cell structures and basic operation conditions [26 - 29].

Parameters	Unit	Value	Reference
Channel length, width, depth	mm	100; 1; 1	[26]
Thickness of bipolar plate	mm	2.5	[26]
Thickness of ADL, AFL, Electrolyte	μm	680; 20 ; 20	[27]
Thickness of CFL	μm	20	[27]
Porosity of ADL, AFL, CFL		0.335; 0.335; 0.335	[27]
Tortuosity of ADL, AFL, CFL		2.5; 2.5; 2.5	[27]
Particle-radii ratio		1	[28]
Electronic-conducting particle radius of ADL, AFL, CFL	μm	1; 0.2; 0.2	[28]
Operating pressure	atm	1	[28]
Operating temperature	K	1073	-
Inlet temperature of fuel and air	K	1073	-
Air composition		21% O_2, 79% N_2	[27]
Fuel composition		98.3% H2, 3.07% H_2O,	[27]
Cell current density	A m^{-2}	3000	-
Heat transfer coefficient between cell and surroundings	W m^{-2} K^{-1}	50	[28]
Contact angles of particles in AFL, CFL	°	15, 15	[27]
Anode and cathode stoichiometry ratio		1.5; 1.5	-
Thermal conductivity of anode, cathode, electrolyte, interconnect	W m^{-1} K^{-1}	6.23; 9.6; 2.7; 30	[28]
Active energy of anode, cathode	kJ mol^{-1}	120; 160	[29]
Reaction order of H_2, H_2O, O_2		0.	[27]
Transfer coefficient of anode, cathode		0.5; 0.5	[26]

Table 2 Source terms.

Source term	Unit
$S_i = \kappa_i \frac{J_i}{n_i F}$ (In anode/cathode)	kg m^{-3} s^{-1}
$S_{\mathrm{T}} = \begin{cases} \frac{I^2}{\sigma_{\mathrm{ele}}^{\mathrm{eff}}} + \frac{I^2}{\sigma_{\mathrm{ion}}^{\mathrm{eff}}} + \frac{\eta_{\mathrm{act}} I}{\delta_{\mathrm{AFL}}} + I\frac{T\Delta S_{\mathrm{c}}}{2\mathrm{F}} - \frac{h_{\mathrm{side}} \cdot (T_{\mathrm{a}} - T_{\mathrm{env}})}{\delta_{\mathrm{a}}} & \text{(In anode)} \\ \frac{I^2}{\sigma_{\mathrm{ele}}^{\mathrm{eff}}} + \frac{I^2}{\sigma_{\mathrm{ion}}^{\mathrm{eff}}} + \frac{\eta_{\mathrm{act}} I}{\delta_{\mathrm{CFL}}} + I\frac{T\Delta S_{\mathrm{c}}}{2\mathrm{F}} - \frac{h_{\mathrm{side}} \cdot (T_{\mathrm{c}} - T_{\mathrm{env}})}{\delta_{\mathrm{c}}} & \text{(In cathode)} \\ \frac{I^2}{\sigma_{\mathrm{ion}}^{\mathrm{eff}}} - \frac{h_{\mathrm{side}}(T_{\mathrm{BP/CH/ELE}} - T_{\mathrm{env}})}{\delta_{\mathrm{BP}}} & \text{(In BP/Channel/electrolyte)} \end{cases}$	W m^{-3}

Table 3. Diffusion coefficients [30].

Parameter	Correlation/Value
Molecular weight of species i	$M_{i,j} = 2(\frac{1}{M_i} + \frac{1}{M_j})^{-1}$
Mean characteristic length of species i and j	$\sigma_{i,j} = \frac{\sigma_i + \sigma_j}{2}$
Diffusion collision integral	$\Omega_D = \frac{1.06036}{\Gamma^{0.15610}} + \frac{0.19300}{\exp(0.47635\Gamma)} + \frac{1.03587}{\exp(1.52996\Gamma)} + \frac{1.76474}{\exp(3.89411\Gamma)}$ $\Gamma = \frac{k_B T}{(\upsilon_i \upsilon_j)^{0.5}}$
Knudsen diffusion coefficient	$D_{i,\mathrm{K}} = \frac{2}{3}(\frac{8RT}{\pi M_i})^{0.5} r_{\mathrm{g}}$
Binary diffusion coefficient	$D_{i,j} = \frac{0.00266T^{1.5}}{PM_{i,j}^{0.5}\sigma_{i,j}^2\Omega_{\mathrm{D}}}$
Effective diffusion coefficient	$D_i^{\mathrm{eff}} = \frac{\varepsilon}{\xi}(\frac{1}{D_{i,j}} + \frac{1}{D_{i,\mathrm{K}}})$
Density of gas mixture	$\rho = \frac{1}{\sum_{i=1}^{N} Y_i/\rho_i}$
Density of species i	$\rho_i = \rho_{i,298\mathrm{K}} \frac{298}{T}$

Table 4 Three selected groups of parameters.

Parameters	$r_{ed,AFL}$	q_{AFL}	φ_{AFL}	δ_{ELE}	$k_{0,a}$	$k_{0,c}$
Case 1	0.2 μm	1	0.5	20 μm	2.17×10^{-3}	3.115×10^{-6}
Case 2	0.15 μm	1.5	0.55	25 μm	2.17×10^{-3}	3.115×10^{-6}
Case 3	0.2 μm	1	0.45	20 μm	1.17×10^{-4}	1.115×10^{-5}

Table 5 Parametric ranges for global sensitivity analysis.

Number	Model input parameters	Nominal value	Range of variation	Unit
1	Particle radii ratios of AFL/CFL (q)	1	±15%	
2	Relative volume fraction AFL/CFL (φ)	0.5	±15%	-
3	Particle radius of electronic conductors of AFL/CFL (r_{ed})	0.2	±15%	μm
4	Thickness of AFL/CFL (δ)	20	±15%	μm
5	Porosity	0.3	±15%	-
6	Thickness of ADL	680	±15%	μm
7	Thickness of BPa /BPc	500	±15%	μm
8	Sherwood number	3	±15%	-
9	Tortuosity	3	±15%	-
10	Channel length	100	±15%	mm
11	Active energy of anode/cathode	150	±15%	J mol^{-1}
12	Pre-exponential factor of anode	5e-4	±15%	-
13	Pre- exponential factor of anode	5e-6	±15%	-
14	Reaction order of H_2	0.5	±15%	-
15	Reaction order of H_2O	0.25	±15%	-
16	Reaction order of O_2	0.25	±15%	-

Table 6 Sensitive degree of 24 parameters.

Sensitive degree	Factors
Very sensitive factors	$r_{ed,CFL}$, q_{AFL}, q_{CFL}, ε_a, ε_c, φ_{AFL}, φ_{CFL}
Rather sensitive factors	$k_{0,c}$, γ_{O_2}, δ_{AFL}, δ_{CFL}, δ_{ELE}
Insensitivity factors	$r_{ed,AFL}$, δ_{ADL}, δ_{BPa}, δ_{BPc}, Sh, τ, L_{cell}, $E_{act,a}$, $E_{act,c}$, $k_{0,a}$, γ_{H_2O}, γ_{H_2}

Table 7 Non-uniform distribution of microscopic structure along the channel length.

		Particle radii ratios of AFL/CFL	Relative volume fraction	Particle radius	Porosity
Case 4	χ	0	0	0	0
	ω	0	0	0	0
Case 5	χ	15%	15%	15%	15%
	ω	15%	15%	15%	15%
Case 6	χ	15%	0	0	0
	ω	0	15%	15%	15%